AIAA 98-3255

Experimental Study of a Nozzle Using Fluidic Counterflow for Thrust Vectoring

Jeffrey D. Flamm
NASA Langley Research Center
Hampton, Virginia

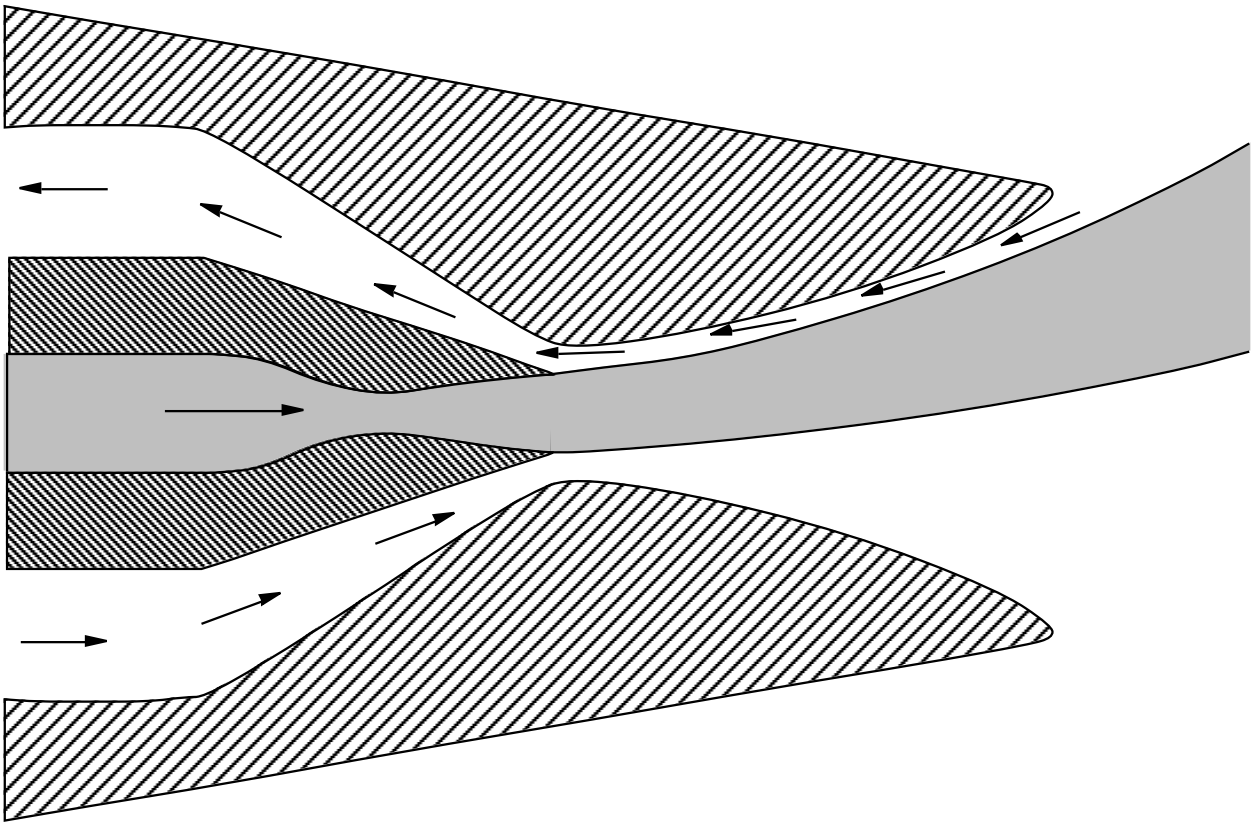

34th AIAA/ASME/SAE/ASEE
Joint Propulsion Conference & Exhibit
July 13-15, 1998 / Cleveland, OH

AIAA98-3255

EXPERIMENTAL STUDY OF A NOZZLE USING FLUIDIC COUNTERFLOW FOR THRUST VECTORING

Jeffrey D. Flamm*
NASA Langley Research Center
Hampton, Virginia

ABSTRACT

A static experimental investigation of a counterflow thrust vectoring nozzle concept was performed. The study was conducted in the NASA Langley Research Center Jet Exit Test Facility. Internal performance characteristics were defined over a nozzle pressure ratio (jet total to ambient) range of 3.5 to 10.0. The effects of suction collar geometry and suction slot height on nozzle performance were examined. In the counterflow concept, thrust vectoring is achieved by applying a vacuum to a slot adjacent to a primary jet that is shrouded by a suction collar. Two flow phenomena work to vector the primary jet depending upon the test conditions and configuration. In one case, the vacuum source creates a secondary reverse flowing stream near the primary jet. The shear layers between the two counterflowing streams mix and entrain mass from the surrounding fluid. The presence of the collar inhibits mass entrainment and the flow near the collar accelerates, causing a drop in pressure on the collar. The second case works similarly except that the vacuum is not powerful enough to create a counterflowing stream and instead a coflowing stream is present. The primary jet is vectored if suction is applied asymmetrically on the top or bottom of the jet.

INTRODUCTION

Studies have shown that thrust vectoring (TV) concepts can provide many benefits to the modern fighter aircraft (figure 1).[1-7] Aircraft combat effectiveness is increased with the addition of TV capability to the aircraft's propulsion system.[1] In close air-to-air combat, TV allows the aircraft to operate in the post stall flight regime. This provides a tactical advantage by increasing aircraft agility and maneuverability.[1,3-7] A further advantage is gained in long range combat by reducing signature and increasing range.[1, 5] Control effectiveness can be augmented with TV at all flight conditions, thereby reducing or eliminating the need for horizontal and vertical tails and, hence, reducing associated drag and radar cross-section. Tail surfaces of a fighter aircraft can account for between 38 and 50 percent of total aircraft drag at transonic flight conditions.[7] The ability to land and take off from short unimproved runways (STOL) is also improved with TV.[1]

Many studies have been conducted on mechanical methods to vector thrust. The techniques used to deflect the flow typically involve moving hinged flaps into the jet exhaust, gimbaling the nozzle, or deflecting the divergent flaps of the nozzle.[8-13] Mechanical thrust vectoring techniques have been demonstrated successfully in three recent flight research programs, the F-15 SMTD, F-18 HARV, and the X-31.[14-16]

Mechanical thrust vectoring techniques have some disadvantages. The mechanical actuators and linkages used to vector thrust add weight and complexity to the aircraft, which in turn increase cost and maintenance requirements. Moveable external flaps, as on the X-31 and F-18 HARV, work against the design goal of creating a stealthy aircraft. These factors have led researchers to investigate novel methods to achieve the same thrust vectoring capabilities without external moving parts. Figure 2 shows a picture of the F-18 HARV thrust-vectoring nozzles, which illustrates the complexity of a mechanical thrust-vectoring method.

A promising area of research is fluidic nozzle control - the use of a secondary air stream to influence the behavior of the primary jet. Fluidic

* Research Engineer, Senior Member AIAA

control requires few or no moving parts in the primary nozzle and several studies have demonstrated the successful use of fluidics to control nozzle flow.[17-20] One technique involves injecting a secondary flow into the primary flow on the nozzle divergent flap. The injected flow creates a disturbance in the primary flow, causing an oblique shock to form, which then turns the primary flow.[17] The fluidic method used in the current study uses a secondary counterflowing stream to vector the primary jet.

The counterflow thrust vectoring concept was first reported by Strykowski and Krothapali.[21] In the counterflow concept, thrust vectoring is achieved by applying a vacuum to a slot adjacent to a primary jet which is shrouded by a suction collar (figure 3). The vacuum creates a secondary reverse flowing stream near the primary jet. The shear layers between the two counterflowing streams mix and entrain mass from the surrounding fluid. The presence of the collar inhibits mass entrainment and the flow near the collar accelerates causing a drop in pressure on the collar, the Coanda effect.[22] If the vacuum is applied asymmetrically to one side of the nozzle or the other, the jet will vector toward the low-pressure region (figure 4).

The unique entrainment characteristics of the countercurrent shear layers are responsible for counterflow flow control.[21] The countercurrent shear layers exhibit higher turbulence and mixing levels than coflowing shear layers.[21, 23, 24] The enhanced mixing characteristics of the counterflow nozzle may have the added benefits of reducing jet noise, jet temperature, and emissions from the nozzle.[25]

The counterflow thrust-vectoring has some limitations. Fluidic concepts in general are bistable and hysteretic in nature.[26, 27] The primary jet tends to attach itself hysteretically to the suction collar at certain conditions (figure 5). This condition eliminates control of thrust vectoring magnitude and, once attached, is difficult to overcome without large changes in flow conditions. This phenomenon has been seen in other studies as well as the current study.[26-28] An additional limitation is the size of the suction collar assembly. The suction collars and suction slots must be kept small to have a minimal impact on aircraft weight and drag.

The purpose of this investigation was to define counterflow nozzle performance over a wide range of operating conditions. Previous studies defined the operating characteristics of the counterflow nozzle over a limited range of conditions.[21, 28-30] Van Der Veer and Schmid studied counterflow nozzles at subsonic exhaust velocities.[28, 30] Strykowski reported results on a counterflow nozzle operating at on-design conditions with supersonic exhaust flow.[21, 29] The data obtained in these previous studies consisted of pressure data and optical measurements of plume angle on subscale, laboratory sized models, A_t = 0.62 in^2 (400 mm^2). The purpose of the current study was to extend the database of counterflow nozzle performance characteristics over a wide range of on- and off-design conditions on a larger scale nozzle, A_t = 3.0 in^2 (1935 mm^2). The current study is the first investigation to define counterflow nozzle performance with accurate force and moment strain-gage balance measurements. The study was conducted at static conditions (no external flow) over a NPR range of 3.5 to 10.0 in the NASA Langley Research Center Jet Exit Test Facility. The effects of suction collar geometry and suction slot height on nozzle performance were examined.[31]

NOMENCLATURE

A_t	nozzle throat area, 3.000 in^2
A_e	nozzle exit area, 5.064 in^2
C	suction collar height, in (figure 8)
F_A	measured axial force, lbs
F_i	ideal isentropic thrust, lbs
F_N	measured normal force, lbs
F_r	measured resultant thrust, lbs
G	measured upper secondary slot height, in.
H	height of primary nozzle exit, 1.125 in.
l	length of primary nozzle, 6.329 in.
L	suction collar length as measured from primary nozzle exit plane, in.
M	Mach number
p	local static pressure, psi
p_0	local total pressure, psi
p_a	atmospheric pressure, psi
$\overline{p}_{cx}$	integral averaged static pressures acting on the suction collar in the x direction, psi
$\overline{p}_{cy}$	integral averaged static pressures acting on the suction collar in the y direction, psi
p_{ej}	ejector supply pressure, psi
p_{slot}	static pressure at suction slot exit, psi

$p_{t,j}$	average total pressure of primary jet, psi
Δp_{slot}	average differential (suction) static pressure at primary nozzle exit (slot), $p_a - p_{slot}$, psi
$T_{t,j}$	average total temperature of primary jet, °R
u	velocity, in/sec
W	width of nozzle, 4.5 in.
w_i	ideal weight flow, lb/sec
w_p	measured weight flow rate of primary jet, lb/sec
w_s	measured weight flow rate of the vacuum lines, lb/sec
x, y, z	Cartesian coordinates
γ	ratio of specific heats, 1.4 for air
δ_p	measured pitch-thrust-vector angle, deg.
$\delta_{p,cv}$	pitch-thrust-vector angle computed from control volume analysis, deg. (eqn 5)
θ	suction collar terminal angle, deg.
ρ	density, slug/ft^3
σ	standard deviation

Subscripts

1	conditions at exit plane of primary nozzle
2	conditions at exit plane of upper suction slot
3	conditions at exit plane of lower suction slot

Abbreviations

1D	one-dimensional
2D	two-dimensional
50s	50% scaled suction collar
50t	50% truncated suction collar
HARV	High-Alpha Research Vehicle
NPR	nozzle pressure ratio, $p_{t,j} / p_a$
NPR_D	design nozzle pressure ratio, 7.824
STOL	short takeoff and landing
SMTD	STOL/Maneuvering Technology Demonstrator
TV	thrust vectoring

Apparatus and Experimental Methods

The study was conducted in the NASA Langley Research Center Jet Exit Test Facility. The following sections will discuss the test facility, dual-flow propulsion system, model hardware, test conditions, and data acquisition and reduction methods.

Jet Exit Test Facility

This facility is used to test nozzle internal performance at static (no external flow) conditions. Tests are conducted in a large room in which the exhaust from the dual flow single-engine simulation system vents to ambient conditions in the test chamber and exits through an acoustically treated duct in the ceiling of the facility. A photograph of a counterflow nozzle installed in the test facility is shown in figure 6. The facility has an air control system that is similar to that of the Langley 16-Foot Transonic Tunnel.[32] A continuous supply of dry high-pressure air is available from a central 5000 psi system. The air is expanded into an 1800 psi reservoir outside the test facility. The air pressure to the dual-flow propulsion simulation system is regulated from within the facility control room.

Dual-Flow Propulsion Simulation System

The counterflow model was tested on a dual-flow propulsion simulation system illustrated by the sketch in figure 7. The system consists of an axisymmetric single-engine propulsion simulation system with dual co-annular ducts mounted on a six component strain gauge balance (NASA balance 1636). Two independent pressurized air streams are supplied to isolated primary and secondary plenum chambers on the test rig. Each air system is instrumented with a multiple critical Venturi system to measure weight flow rate and is capable of providing air at a rate of 18 and 25 lb/sec.[33] A steam heat exchanger in each air system can be used to regulate air flow temperature between 65°F and 90°F immediately upstream of the test nozzle. The high pressure air transitions from the non-metric to metric (supported by the balance) part of the test rig through two pairs (one pair for primary flow and one pair for secondary flow) of semi-rigid, stainless-steel, 's' shaped tubes (S-tubes). The S-tubes are designed to minimize the balance tares and axial momentum transfer caused by the high pressure air crossing the metric/non-metric break on the test rig. The primary air supply passes from the primary plenum to an annular duct located on the test-stand centerline through eight equally spaced sonic nozzles. The flow then passes through a circular duct to a transition section (round-to-rectangular) and choke plate before entering the rectangular instrumentation section. The choke plate acts as a flow straightener. From the instrumentation section, the flow then enters the primary nozzle. The secondary flow plenum and duct system were not used for the current study. The secondary air system was used to power an ejector pump, described below, which provided suction for the counterflow nozzle.

Model Description

The model consisted of a two-dimensional (2D) primary nozzle and two secondary passages positioned above and below the 2D convergent-divergent primary nozzle. The model was symmetric about the *x-y* and *x-z* planes. A sketch of the model is shown in figure 8. A photograph of a typical nozzle configuration is shown in figure 9 with the near sidewall removed. The primary nozzle design NPR was 7.824 (M = 2.0) and was a larger scale (220%) version of the nozzle tested in reference 29. There were two geometric variables tested on the model: secondary slot height, G, and suction collar length, L. The slot height was varied by translating the suction collar in the vertical plane of the model. The three secondary slot heights were nominally G = 0.464, 0.222, and 0.110 in.

Three suction collar designs, which varied collar length and shape, were tested. The baseline collar length was 7.957 in. and is denoted as the 100% collar and was obtained by scaling (220%) the collar tested in reference 29. The second collar design was obtained by truncating the 100% collar at 50% of its length and is denoted as the 50% *truncated* (50t) collar. This geometry change was accomplished by removing the suction collar extensions as shown in figure 8. The third collar design was obtained by scaling the 100% collar by 50% and is denoted as the 50% *Scaled* (50s) collar.

Ejector Pump

The vacuum source for the secondary suction flow or counterflow jet was provided by an ejector pump mounted downstream of the model test rig (figure 6). The low pressure side of the ejector was connected to the upper suction plenum of the counterflow model by two flexible 1 inch vacuum lines. The ejector was powered with high pressure air from the Jet Exit facility's secondary air system and was connected using two 1 inch high pressure airlines. Ejector supply pressure was varied from "off" to 966 psi, the maximum allowable operating pressure, to throttle the vacuum pressure. The nozzle lower secondary flow slot was allowed to entrain ambient air (figure 4).

Instrumentation

Forces and moments on the model were measured using a six-component strain gauge balance (NASA balance 1636). The balance load ranges and estimated accuracy for each component are listed in table 1. Since the model was symmetric about the *x-y* and *x-z* planes, significant rolling moment, yawing moment, and side force measurements were not expected.

The model was instrumented with 130 surface static pressure taps on the internal and external surfaces of the primary nozzle, the internal surface of the suction collars, and in the upper and lower suction plenums. The model static pressures were measured using electronic pressure transducers with a range of 15 psid. The accuracy of the pressure transducers as given by the manufacturer was ±0.1 percent of full scale.

The ejector pump was instrumented with four static pressure taps in the ejector plenum. These pressures were used to monitor the ejector supply pressure. They were measured by four externally mounted pressure transducers with a range of 2000 psia and accuracy of ±0.1 percent full scale.

The weight flow rate of the air supplied to the primary nozzle, w_p, was measured by a multiple critical Venturi system located upstream of the S-tubes. The multiple critical Venturi's have been calibrated to an accuracy of 0.1 percent. Reference 33 describes the multiple critical Venturi system in further detail.

The flow rate of the secondary (vacuum) supply lines was measured using turbine flow meters. The accuracy of the turbine flow meters was ±0.5 ft^3/sec.

The primary jet total pressure, $p_{t,j}$, was obtained by mounting two rakes with a combined total of five Pitot probes in the instrumentation section upstream of the primary nozzle (figure 7). The pressures were measured by individual 250 psid pressure transducers with an accuracy of ±0.06 percent of full scale. The five individual readings were then averaged to obtain $p_{t,j}$. The primary jet total temperature, $T_{t,j}$, was obtained by averaging measurements from two thermocouples also mounted in the instrumentation section. The maximum temperature range of the thermocouples was 32 to 1382 degrees Fahrenheit. The accuracy of the thermocouples as given by the manufacturer was ±4 °F. The ambient pressure, p_a, was measured with a

15 psia pressure transducer with an accuracy of ±0.1 percent of full scale.

Data Acquisition and Reduction

All data in this study were obtained at the rate of 10 frames per second and averaged over 5 seconds to obtain steady-state values. The basic performance parameters presented in this report are: resultant thrust ratio, F_r/F_i,; primary flow discharge coefficient, w_p/w_i; and pitch-thrust-vector angle, δp. Reference 34 presents a detailed description of the data reduction procedures used in this study.

A series of corrections were applied to the balance data to obtain final balance force and moment data. The data were initially corrected for model weight tares and interactions of the balance components. It was necessary to further calibrate the balance in the test stand to account for additional restraints on the balance due to high-pressure air S-tubes and vacuum lines bridging the metric break. Although the S-tube arrangement and flexible vacuum lines were designed to minimize interactions with the balance, small tares still exist on all balance components. A description of the calibration procedures for the facility can be found in reference 32.

The uncertainties of the computed data reduction quantities are listed in table 2. References 40 and 41 give a detailed description of the method used to determine the data uncertainty.

Test Conditions

The model was tested over an NPR range of 3.5 to 10. Secondary nozzle suction pressure was obtained by setting the ejector supply pressure, p_{ej}, and was limited by the capability of the ejector vacuum system. Secondary nozzle suction pressure, Δp_{slot}, varied from approximately Δp_{slot} = 0.5 to 7.8 psi. Suction was only applied to the upper secondary slot; the lower secondary slot was left open to atmosphere. The air flow stagnation temperature was maintained at approximately 80°F. Geometric variables included suction slot height, G, and suction collar length, L. The test matrix is presented in table 3.

RESULTS AND DISCUSSION

Nozzle Performance without Counterflow

The following section presents the basic nozzle performance characteristics with the ejector vacuum system turned off, $p_{ej} = p_a$. The upper and lower secondary passages were open to ambient conditions. As such, they acted as ejectors and provided additional flow to the nozzle system via the pumping action of the primary jet.

Figure 10 shows the effect of suction collar geometry on nozzle performance as a function of NPR. The primary flow discharge coefficient generally showed no effect due to suction collar geometry without counterflow. This was true throughout the entire test both with and without the counterflow system active.

With the counterflow system inactive, pitch-thrust-vector angle showed no effect due to suction collar geometry. However, each of the three collar geometries generally produced 1° to 2° positive pitch vectoring, δp, even though the suction system was turned off and no counterflow was present. The positive pitch vectoring is probably a result of asymmetric entrainment of flow by the primary jet through the upper and lower suction slots. The lower suction slot was left open to atmosphere to freely entrain flow at all times during the test. The upper suction slot, connected to the ejector suction system, was also open to atmosphere when the suction system was turned off. However, the ejector system remained connected at all times and added blockage to the upper suction slot path to atmosphere. The ejector system added approximately twenty feet of both rigid and flexible airline between the upper secondary plenum and the ambient conditions of the test chamber (figure 6). In contrast, the lower secondary plenum was open to the ambient conditions of the test chamber at the base of the model.

The resultant thrust ratio followed trends similar to those reported for previously tested convergent-divergent nozzles.[36-38] The resultant thrust ratio increased with increasing NPR to a maximum value at NPR = 8.0 and then generally leveled off or decreased near NPR = 10. A convergent-divergent nozzle is most efficient (maximum value of F_r/F_i) at the design nozzle pressure ratio NPR_D. At NPR_D, the flow is fully

expanded and there are no shocks or separation within the nozzle. At NPRs below design, the flow is overexpanded and a shock forms within the nozzle or at the exit plane and recompresses the flow. The losses from the shock and possible attendant flow separation decrease the resultant thrust ratio. At NPRs above design, the nozzle is underexpanded and the flow continues to expand outside the nozzle in an expansion fan. Thus, all of the available energy is not extracted from the flow before it exits the nozzle, which results in a decrease in resultant thrust ratio. From the results shown in figures 10 and 11, it appears that the thrust performance of the counterflow nozzle (includes suction collar) with no counterflow is dominated by the primary nozzle performance since resultant thrust ratio tended to peak at a NPR close to the primary nozzle NPR_D of 7.824 for the two 50% collars. Apparently the primary nozzle is not pumping enough external flow to fill the suction collar portion of the nozzle. The greater length of the 100% collar appears to improve the pumping action of the primary nozzle. The peak in resultant thrust ratio occurred at a value of NPR ≥ 10 for the 100% collar.

The resultant thrust ratio was significantly affected by collar geometry for a given slot height, *G*. The two short (50%) suction collars had 0.02 to 0.05 higher resultant thrust ratios than the long (100%) suction collar. The decrease in efficiency of the 100% collar may be caused by an inrease in base drag due to its larger size. The 50% scaled collar was generally the most efficient collar design at all NPRs and slot heights tested. The resultant thrust ratio of the 50% truncated collar was typically 0.5% to 1.0% lower than that of the 50% scaled collar at all NPRs and slot heights.

Figure 11 shows the effect of suction slot height on nozzle performance without counterflow. For the case of no counterflow ($p_{ej} = p_a$), slot height generally had a negligible effect on resultant pitch-thrust-vector angle, δ_p, and flow discharge coefficient, w_p/w_i. One notable exception to this trend occurred on the configuration with the 50% truncated collar, G = 0.222 in. at NPR = 4.0. The resultant pitch-thrust-vector angle, δp, was -12.9 degrees for this condition. The centerline pressure distribution for the suction collar, shown in figure 12, at NPR= 4 indicates that the surface pressure distribution on the upper suction collar was pumped down by the primary jet, whereas the pressure distribution on the lower suction collar was not. It can also be noted that the internal surface pressure distributions for the primary nozzle indicate a shock (and possible separation) on the lower surface, but not on the upper surface (figure 13). The asymmetric (oblique) shock in the primary nozzle resulted in pitch vectored primary exhaust flow toward the upper suction collar. The closer proximity of the primary jet to the upper suction collar surface caused stronger entrainment (pumping), lower pressures on the upper suction collar (see figure 12) and a large negative pitch vector angle (see figure 11). The primary nozzle is overexpanded at an NPR = 4.0 (NPR_D = 7.824) and this caused the shock inside the primary nozzle. The asymmetric character of the shock was probably caused by slightly different back pressures at the primary nozzle (and slot) exit as a result of the different upper and lower slot blockages discussed previously. Similar results might be expected at NPR < 4.0 (not tested) since the primary nozzle would be even more overexpanded at lower NPR.

Nozzle Performance with Counterflow

The following section presents the basic nozzle performance characteristics with the ejector vacuum system turned on. During examination of these data, it is important to remember that counterflow (suction) was applied to only the upper secondary passage (slot). The lower passage was open to ambient conditions. Normal counterflow operation is indicated in figure 4.

NPR Effects

Figures 14 and 15 present typical plots of the effect of NPR on nozzle performance and centerline pressure distributions with counterflow for the configuration with a slot height G = 0.469 in. and the 50% truncated collar. The data in figure 14 are plotted against the term Δp_{slot}, an indicator of the suction being generated by the ejector system. For clarity, multiple hysteresis loops (discussed later) have been eliminated from the data presented in figure 14. Except for special cases, thrust vector angle magnitude increased with increasing Δp_{slot}. For example, increasing Δp_{slot} from 0.84 to 4.48 at NPR = 8 caused an increase in negative pitch-thrust-vector angle from -.10 deg. to -6.7 deg. As shown in figure 15, increasing Δp_{slot} (upper slot only) decreased pressure on the entire upper collar surface

(except at the trailing edge) and this pressure-area term was the cause of increased δ_p magnitude.

Except for special cases which will be discussed later, the magnitude of δ_p decreased with increasing NPR for a given value of Δp_{slot}. These results were caused by increasing momentum flux per unit area of the primary jet as NPR increases. The momentum flux is given by:

$$\rho u^2 = \left(\gamma p M^2\right)_1 \quad (1)$$

The axial force, F_A, of the primary jet is proportional to the momentum flux. The pitch-thrust-vector angle is inversely proportional to the axial force acting on the model.

Similar to the results with counterflow off, NPR = 8.0 was typically the most efficient NPR for each counterflow-on configuration as measured by resultant thrust ratio, F_r/F_i. This condition corresponds closest to the design NPR (7.824) for the primary nozzle. Except for special cases, F_r/F_i for all NPRs decreased with increasing Δp_{slot} (and consequently increasing pitch-thrust-vector angle magnitude). The loss in efficiency may be due to several factors. One possible cause may be an increase in base drag with increasing Δp_{slot}. As the suction rate is increased, the pressures along the upper collar surface are reduced to below ambient and thus, cause pressure drag on the nozzle. Another possible cause of the reduction in efficiency may be the result of less mass flow exiting the nozzle than was introduced by the primary nozzle. With the counterflow system on, some mass flow from the primary jet may be drawn into the suction passage, thereby reducing the amount of mass flow available to produce thrust.

Effect of Slot Height

Figure 16 presents the effect of slot height on nozzle performance at NPR = 8 for the 100% collar configurations. For a given Δp_{slot} , pitch-thrust-vector angle magnitude increased with increasing slot height, G, when the jet was not attached to the collar (to be discussed later). This trend was also evident at all other NPRs tested. These data support the findings reported in reference 29. In reference 29, an effect due to slot height was found for $0.27 \le G/H \le 0.38$. The ratio of G/H for the current study is $0.098 \le G/H \le 0.412$.

When the jet was not attached to the suction collar, the thrust efficiency, F_r/F_i, improved as the slot height was reduced at a given Δp_{slot}. This trend was evident for all configurations at all NPRs tested.

Effect of Collar Geometry

Figure 17 presents the effect of collar geometry on nozzle performance as a function of Δp_{slot} at NPR = 8.0 while holding slot height fixed at G = 0.222 in. When the jet was not attached to the collar, the 100% collar generally provided more pitch-thrust-vectoring for a fixed Δp_{slot}, while the two 50% collars performed similarly. At NPR = 8.0, Δp_{slot} = 3.0 psi., the two 50% collars produced approximately 3 degrees of pitch-thrust vectoring, whereas the 100% collar produced 6 degrees of pitch-thrust vectoring. This result was expected because the 100% collar has twice as much projected surface area as the two 50% collars in the xz-plane on which pressure can act to produce a normal force.

Similar to the results shown in figure 10 for counterflow off, the thrust efficiency, F_r/F_i, of the 100% collar was generally lower than that of the two 50% collars when the jet was not attached to the collar. At NPR =8.0, the thrust efficiency of the 100% collar was typically 2.5 percent lower than the 50% collars. The two 50% collars performed similarly with increasing Δp_{slot}.

Jet attachment

There are several special cases in which the nozzle did not follow the trends indicated above. These special cases were caused by the primary jet plume attaching to one or both of the suction collars at some test conditions.

Increasing the ejector supply pressure, p_{ej}, and consequently the vacuum at the suction slot, Δp_{slot}, caused the primary jet to attach to the upper suction collar for some configurations at some test conditions while remaining unattached from the lower collar (see figure 5). This asymmetric jet attachment is indicated by the δp and p_{ej} data shown in figure 18. Jet attachment is indicated by a large discontinuity in δp with increasing Δp_{slot}. When the jet attached to the suction collar, the pitch-thrust-

vector angle, δp, would generally jump to a value near the suction collar terminal angle, θ (figure 8). An example of this phenomenon is evident in figure 18. The last condition at which the jet was not attached to the upper collar was at Δp_{slot} = 3.29 psi, which produced δp = -8.78 deg. Increasing the ejector supply pressure slightly to p_{ej} = 591 psi and hence increasing the vacuum at the slot caused the jet to attach to the collar and reach equilibrium at Δp_{slot} = 7.79 psi and δp = -26.7 deg.

It is also helpful to examine the collar centerline pressure distributions for the jet attached case (figure 19). The pressure distribution along the lower collar surface remained flat at near ambient conditions for all suction rates, indicating that the lower collar was not affected by the primary jet. This pressure distribution on the lower collar was typical for all configurations except when the primary jet was attached to both collars, as discussed later. The upper collar pressure distribution was initially flat and near ambient along the length of the collar when the ejector was off. As suction increased, the counterflow process began and the pressure decreased linearly along the collar surface until approximately x/l = 1.25. Beyond x/l = 1.25, the pressure recovered to near ambient conditions toward the end of the collar. Similar trends were seen for all freely vectoring (unattached) cases. However, the starting location and length of pressure recovery were dependent on the configuration. As the amount of suction was increased further, the pressure distribution suddenly decreased down the length of the collar (indicating jet attachment). The pressure did not recover to near ambient conditions until the very end of the collar. A jet unattached case is illustrated by the pressure distributions shown in figure 15. The pressure distribution was flat and near ambient with the ejector system off. As Δp_{slot} increased, the suction collar static pressures decreased linearly along the collar until approximately x/l = 1.25 and then recovered gradually to near ambient conditions at the end of the collar. The sharp decrease in the pressures on the collar surface at some value of Δp_{slot} is not present for the jet unattached case (compare figures 15 and 19).

Jet attachment was a hysteretic phenomenon. Once the jet was attached to the collar, simply reducing the ejector supply pressure to reduce Δp_{slot} back to the value at which jet attachment occurred was not sufficient to release the jet from the collar. It was generally necessary to turn the ejector off and even reduce the primary jet NPR to release the jet from the collar. Once the jet attached to the upper suction collar, changes in the ejector supply pressure had little effect on Δp_{slot}, jet attachment, or pitch-thrust-vector angle. The p_{ej} versus Δp_{slot} plot shown in figure 18 illustrates the hysteresis problem. At NPR = 8, the last condition at which the jet was not attached to the upper collar was at p_{ej} = 575 psi, Δp_{slot} = 3.29 psi, δp = -8.78 deg. Increasing the ejector supply pressure, and hence the vacuum at the slot, to p_{ej} = 591 psi caused the jet to attach to the collar and reach equilibrium at Δp_{slot} = 7.79 psi and δ_p = -26.7 deg. Turning the ejector off, $p_{ej} = p_a$, reduced the slot pressure slightly to 7.10 psi, but the jet remained attached and δ_p remained close to -27 degrees. The 100% collar suffered from jet attachment more than the other collar geometries tested. This collar geometry experienced jet attachment at all gap heights tested. The 50% truncated collar only experienced jet attachment at the smallest gap height tested (G = 0.110 in.).

Jet attachment is a result of the Coanda effect, which is the propensity of a fluid flowing near a solid surface to attach itself to the surface. As the jet leaves the primary nozzle it forms a turbulent shear layer and entrains surrounding fluid. As the fluid near the solid surface is entrained, it is accelerated, which results in a reduced static pressure near the surface. The reduced static pressure tends to pull the jet toward the surface and accelerates the shear layer more, thus further reducing the static pressure on the surface. If the solid surface is long enough, the jet eventually attaches to the surface and cuts off the path for entrainment from the surrounding fluid. [22, 26, 30, 35]

At conditions when the primary nozzle was underexpanded (NPR > NPR_D), very little pitch vectoring capability was provided by some configurations. An example is shown in figure 20 for the 100% collar, G = 0.110 in. configuration at NPR = 10. The magnitude of pitch-thrust-vector angle never exceeded 1.1 deg. for this case. The centerline pressure distributions along the upper and lower suction collar surfaces for this configuration indicate that the primary jet impinged (attached) on both the upper and lower collar surfaces and then separated from the collar further downstream (figure 21). Jet

attachment to both suction collar surfaces is illustrated in figure 20. This phenomena was evident on the two smallest slot heights (G = 0.222 and 0.110 in.) on the 100% collar and the 50% truncated configurations at NPR =10. The larger wall curvature for the 50% scaled collar apparently moves the suction collar surface far enough away from the primary jet such that jet impingement on the lower surface does not occur for this configuration over the NPR range tested. Additionally, this phenomenon (jet attachment to both suction collar surfaces) did not occur for the largest slot height tested (G = 0.464 in.) with any of the suction collars installed. Again, the suction collar surface was too far from the primary jet for attachment to occur. These results are consistent with convergent - divergent nozzle theory. At underexpanded conditions, the primary jet goes through an expansion fan at the nozzle exit and the plume diameter increases toward the suction collar. As the gap height is reduced, the collar is moved closer to the primary jet plume until the primary jet interacts with the collar and ultimately attaches to it. The suction collars now act as new divergent flaps at a new highly overexpanded condition. Because the nozzle is now highly overexpanded, the flow separates further downstream and the collar pressures return to near ambient conditions. At NPR > 10, where the primary plume height would be expected to be larger, jet attachment may occur on the upper and lower collar surfaces for the 50% scaled collar and the large slot height (G = 0.464 in.) configurations as well. When the jet impinges on the collar, the flow passage is closed off and counterflow is not possible. Increasing Δp_{slot} (upper slot only) only lowers the pressure over the region ahead of the point where the jet impinges on the collar (see figure 21).

Secondary weight flow measurements

Secondary weight flow measurements were obtained in a second counterflow nozzle test entry. These measurements indicate that the counterflow concept does not necessarily depend upon the generation of a secondary counterflowing shear layer to generate thrust vectoring. Measurements of the weight flow in the secondary (vacuum) lines, w_s, indicated that a secondary coflowing stream was present at some test conditions.

Figure 22 shows the secondary to primary weight flow ratio, w_s/w_p, and pitch-thrust-vector angle, δ_p, versus Δp_{slot} for the 100% collar, G = .459 in. configuration at NPRs 10 and 8. Values of w_s/w_p greater than zero indicate the presence of counterflow. Values of w_s/w_p less than zero indicate the presence of coflow. The magnitude of the secondary weight flow, w_s, was typically less than 1% that of the primary weight flow, w_p. At NPR = 8, the secondary weight flow indicated counterflow at $\Delta p_{slot} > 1.0$ psi until $\Delta p_{slot} \approx 3$ psi after which the jet attached to the suction collar. The jet vectored freely over the range $0.5 < \Delta p_{slot} < 3.0$ psi reaching a maximum of 8.1 degrees in pitch-thrust-vector angle magnitude. At NPR = 10, the secondary weight flow remained in the coflow direction across the entire range of Δp_{slot} tested. However, the jet still vectored freely between $1.0 < \Delta p_{slot} < 4.0$ psi, reaching a maximum magnitude of 5 degrees. The fact that the primary jet vectored without the presence of counterflow indicates that counterflow is not the primary means by which the jet is vectored.

Control Volume Analysis

In order to better understand the counterflow nozzle operating characteristics, it is desirable to develop a method to predict thrust-vectoring performance based on geometric variables and flow conditions. In a previous study, Van Der Veer deduced a similarity parameter, which predicted thrust vectoring angle.[28] This study was performed on a subsonic jet and used optical techniques to determine thrust vector angle. The similarity parameter is of the form:

$$\delta_p \propto \frac{\Delta p_{slot}}{\left(\gamma M^2 p\right)_1} \frac{L}{H} \qquad (2)$$

A subsequent study also applied this parameter to a small scale supersonic nozzle operating on design.[29] Figure 23 shows the data obtained in the current study plotted using relationship (2) at all NPRs tested. As shown, this parameter did not correlate the data from this investigation (which included off-design points) very well.

Hunter and Wing performed a control volume analysis of a counterflow model that produced a parameter, which improved the correlation between experimental and predicted data.[39] The basic assumptions used in the analysis

were: (1) fixed rigid control volume, (2) frictionless walls, (3) 2D system, (4) steady flow, and (5) uniform 1D velocities. From this analysis, the pressure forces and momentum fluxes acting on the model are:[39]

$$F_A = \begin{Bmatrix} (p_1 - p_a)HW + (p_2 - p_a)GW \\ +(p_3 - p_a)GW + (\bar{p}_{cx} - p_a)CW \\ +\rho_1 u_1^2 HW + \rho_2 u_2^2 GW + \rho_3 u_3^2 GW \end{Bmatrix} \quad (3)$$

$$F_N = \bar{p}_{cy} LW \quad (4)$$

where the subscripts 1, 2, 3 denote conditions at the primary exit, upper suction slot, and lower suction slot, respectively (see figure 8 for definition of geometric variables). The terms $\bar{p}_{cx}$ and $\bar{p}_{cy}$ are the integral averaged static pressures acting on the suction collar in the *x* and *y* directions, respectively.

Recasting equations (3) and (4) in terms of measured quantities yields:

$$\delta_{p,cv} = \tan^{-1}\left\{ \frac{\bar{p}_{cy}}{p_1}\frac{L}{H} \left[\begin{array}{l} 1 + \dfrac{2\gamma}{\gamma-1}\left[\left(\dfrac{p_{01}}{p_1}\right)^{\frac{\gamma-1}{\gamma}} - 1\right] \\ + \dfrac{p_2}{p_1}\left[\dfrac{2\gamma}{\gamma-1}\left(\dfrac{p_{o2}}{p_2}\right)^{\frac{\gamma-1}{\gamma}} - \dfrac{\gamma+1}{\gamma-1}\right]\dfrac{G}{H} \\ + \dfrac{p_3}{p_1}\left[\dfrac{2\gamma}{\gamma-1}\left(\dfrac{p_{03}}{p_3}\right)^{\frac{\gamma-1}{\gamma}} - \dfrac{\gamma+1}{\gamma-1}\right]\dfrac{G}{H} \\ + \dfrac{\bar{p}_{cx}}{p_1}\dfrac{C}{H} - \dfrac{p_a}{p_1}\dfrac{H+2G+2C}{H} \end{array} \right] \right\}^{-1} \quad (5)$$

The numerator of equation (5) is similar to the parameter in relationship (2). Relationship (2) can be viewed as an approximation of equation (5) in which the effects of momentum and pressure forces generated by the secondary flows and the primary flow pressure force are neglected and the pressure field generated on the suction collars is estimated by the gage pressure in the suction slot.

Figure 24 shows the data computed from the force and moment balance measurements from this study at all NPRs tested plotted against the pitch-thrust-vector angle computed using equation (5). The data correlation is linear with little scatter, but pitch-thrust-vector angle is slightly under predicted.

Observing that the pressure force and momentum fluxes associated with the secondary flows are small compared to the other terms in equation (5), the corresponding terms can be eliminated from equation (3):

$$F_A = \begin{Bmatrix} (p_1 - p_a)HW + \cancelto{0}{(p_2 - p_a)GW} \\ +\cancelto{0}{(p_3 - p_a)GW} + (\bar{p}_{cx} - p_a)CW \\ +\rho_1 u_1^2 HW + \cancelto{0}{\rho_2 u_2^2 GW} + \cancelto{0}{\rho_3 u_3^2 GW} \end{Bmatrix} \quad (3)$$

And equation (5) can be simplified to:

$$\delta_{p,cv} \cong \tan^{-1}\left\{ \frac{\bar{p}_{cy}}{p_1}\frac{L}{H} \left[\begin{array}{l} 1 + \dfrac{2\gamma}{\gamma-1}\left[\left(\dfrac{p_{01}}{p_1}\right)^{\frac{\gamma-1}{\gamma}} - 1\right] \\ + \dfrac{\bar{p}_{cx}}{p_1}\dfrac{C}{H} - \dfrac{p_a}{p_1}\dfrac{H+2C}{H} \end{array} \right] \right\}^{-1} \quad (6)$$

Figure 25 shows the simplified control volume estimates from equation (6) plotted against the measured pitch-thrust-vector angle. The data still collapse linearly using the simplified control volume analysis. The assumption that the secondary pressure forces and momentum fluxes were negligible is valid. However, the primary flow pressure force and integral-averaged collar-pressure forces are of the same order and cannot be eliminated from equation (6). Note that in equation (6), pitch-thrust-vector angle is no longer explicitly a function of suction slot height, *G*. As discussed previously, the pitch-thrust-vector angle did depend on *G*. Equation (6) collapses the data because the influence of varying slot height is still present in the integrated collar pressure terms of the equation.

The data shown in figure 25 can be approximated by the line:

$$\delta_p = 0.8857\ \delta_{p,cv,\ eqn\ 6} + 1.143 \quad (7)$$

Ideally, the measured pitch-thrust-vector angle and the computed angle would correspond on a one-to-one basis. As discussed previously, the initial pitch-thrust-vector angle was between 1 and 2 deg. with counterflow off. This initial bias from zero may account for part of the discrepancy between the measured and predicted pitch-thrust-vector angle, specifically the intercept of 1.143 in equation (7). Further differences between the measured and

estimated pitch-thrust-vector angle may be the result of additional effects not properly modeled by the control volume analysis such as viscous or 3D effects.

CONCLUDING REMARKS

The purpose of the current study was to investigate counterflow nozzle performance characteristics over a wide range of both on-and off-design conditions on a model that accurately simulated a full-scale nozzle configuration. Accurate force and moment balance measurements were obtained to quantify nozzle performance. The study was conducted over a nozzle pressure ratio range of 3.5 to 10.0. Three collar geometries were tested, an 8-inch long collar (100%), the 8-inch collar truncated at 50 percent length (50% truncated), and the 8-inch collar scaled by 50 percent (50% scaled). Three suction slot heights were also tested, nominally 0.465, 0.222, and 0.110 in.

The basic nozzle performance for the model without counterflow was defined. Pitch-thrust-vector angle generally was not affected by variations in slot height or collar geometry. The resultant thrust ratio with counterflow off followed trends reported for previously tested convergent-divergent nozzles; peak thrust performance occurred near NPR_D. The resultant thrust ratio was not affected by slot height variations. The 100% collar was the least efficient collar configuration at all NPRs, typically between 2.0% to 5.0% lower than the 50% scaled collar. The 50% scaled collar was generally the most efficient collar, typically 0.5% to 1.0% higher than the 50% truncated collar. The primary-flow discharge coefficient was constant throughout the entire test and was approximately 0.997.

With counterflow on, the primary jet attached hysteretically to the upper suction collar on some configurations. Jet attachment was caused by the Coanda effect and was most evident on the 100% collar. Truncating the collar reduced the tendency of the jet to attach to the collar. Decreasing slot height increased the likelihood of jet attachment. The smallest slot height, 0.110 in., configurations were most susceptible to jet attachment. For a given suction rate as defined by the differential static pressure at the primary nozzle exit, pitch-thrust-vector angle increased with increasing slot height when the jet was not attached to the collar. The 100% collar produced a larger pitch-thrust-vector angle magnitude at a given suction rate than the two 50% collars. Resultant thrust ratio increased as slot height decreased.

Secondary (vacuum) line weight flow measurements were made. The magnitude of the secondary weight flow was small compared to that of the primary jet (less than 1%). The data indicate that the generation of a countercurrent shear layer is not necessary to vector the primary jet using the suction technique.

The data were examined using a control volume analysis and a correlation parameter was identified. The effects of the secondary (counterflowing) pressure and momentum fluxes were found to be negligible from this analysis. It was also found that the primary jet pressure forces could not be neglected.

The counterflow concept is a viable method for generating vectored thrust on an aircraft. Pitch-thrust-vector angles in excess of 15 degrees (jet unattached) were demonstrated in this study. The counterflow concept (and fluidic concepts in general) has many potential benefits over conventional mechanical thrust vectoring techniques, including reduced weight and complexity, which in turn reduce aircraft cost and increase reliability. The introduction of a secondary counterflowing air stream into the nozzle also increases mixing which may reduce jet noise, plume temperature and emissions from the aircraft engine. The counterflow nozzle also offers advantages over fluidic injection thrust vectoring techniques due to its relatively low secondary flow rates as illustrated in the simplified control volume analysis and secondary weight flow measurements presented in this study. For the counterflow nozzle to be practical for use on an aircraft, the suction collar geometry and slot heights must be kept as small as possible to reduce structure and base drag on the aircraft. However, this investigation showed that small slot heights (moving the suction collar closer to the primary jet) were more prone to jet attachment due to the Coanda effect. Further studies are necessary to better understand the jet attachment phenomena.

REFERENCES

1. Bitten, R.; and Selmon, J.: Operational benefits of Thrust Vector Control (TVC). *High-Angle-of-Attack Technology*, *Volume I*, Joseph R. Chambers, William P. Gilbert, and Luat T. Nguyen, eds., NASA CP-3149, Part 2, 1992, pp. 587-601.

2. Herbst, W. B.: "Future Fighter Technologies," *J. Aircr.*, vol. 17, no. 8, August 1980, pp. 561-566.

3. Herrick, P. W.: *Propulsion Influences on Air Combat.* AIAA-85-1457, July 1985.

4 Nguyen, Luat T.; and Gilbert, William P.*: Impact of Emerging Technologies on Future Combat Aircraft Agility.* AIAA-90-1304, May 1990.

5. Herrick, P. W.: *Air Combat Payoffs of Vectoring/Reversing Exhaust Nozzles.* AIAA-88-3239, July 1988.

6. Costes, Philippe*: Investigation of Thrust Vectoring and Post-Stall Capability in Air Combat.* AIAA-88-4160-CP, 1988, pp. 893-905.

7. Capone, F. J.: *The Nonaxisymmetric Nozzle - It is for Real.* AIAA-79-1810, August 1979.

8. Berrier, B. L.; and Re, R. J.: *A Review of Thrust-Vectoring Schemes for Fighter Aircraft.* AIAA-78-1023, July 1975.

9. Re, Richard J.; and Leavitt, Laurence D.: *Static Internal Performance Including Thrust Vectoring and Reversing of Two-Dimensional Convergent-Divergent Nozzles.* NASA TP-2253, February 1984.

10. Bare, Anne E.; and Reubush, David E.: *Static Internal Performance Including of a Two-Dimensional Convergent-Divergent Nozzle with Thrust Vectoring.* NASA TP-2721, July 1987.

11. Asbury, Scott C.; and Capone, Francis J.: *Multiaxis Thrust-Vectoring Characteristics of a Model Representative of the F-18 High-Alpha Research Vehicle at Angles of Attack from 0° to 70°.* NASA TP-3531, December 1995.

12. Lamb, Milton; and Bangert, Linda S.: *Internal Performance of a Lightweight Multiaxis Thrust Vectoring and Reversing Nozzle with Flow Splay Capability.* NASA TP-3571, May 1996.

13. Berrier, Bobby L.; and Taylor, John G.: *Internal Performance of Two Nozzles Utilizing Gimbal Concepts for Thrust Vectoring.* NASA TP-2991, 1990.

14. Bursey, R.; Dickinson, R.: *Flight Test Results of the F-15 SMTD Thrust Vectoring/Thrust Reversing Exhaust Nozzle.* AIAA-90-1906, July 1990.

15. Regenie, Victoria; Gatlin, Donald; Kempel, Robert; and Matheny, Neil*: The F-18 High Alpha Research Vehicle: A High Angle-of-Attack Testbed Aircraft.* NASA TM-104253, 1992.

16. Knox, Fred; and Scellenger, Harvey: *X-31 Flight Test Update.* AIAA-92-1035, February 1992.

17. Wing, David, J.: *Static Investigation of Two Fluidic Thrust-Vectoring Concepts on a Two-Dimensional Convergent Divergent Nozzle.* NASA TM-4574, December 1994.

18. Federspiel J.; Bangert, Linda L.; Wing, D.; and Hawkes, T.: *Fluidic Control of Nozzle Flow - Some Performance Measurements.* AIAA 95-2605, July 1995.

19. Porzio, A. J.; and Franke, M. E.: "Experimental Study of a Confined Jet Thrust Vector Control Nozzle," *Journal of Propulsion and Power*, vol 1., no. 5, September 1989, pp. 596 - 601.

20. Fitzgerald, R. E.; and Kampe, R. F.*: Boundary Layer TVC for Missile Applications.* AIAA-83-1153, June 1983.

21. Strykowski, P. J.; and Krothapalli, A.: *The Countercurrent Mixing Layer: Strategies for Shear-Layer Control.* AIAA 93-3260, July 1993.

22. Coanda, H.: Procédé Propulsion Dans Un Fluide. Brevet Invent. Gr C1.2, no. 762688 Républic Fran. 1932.

23. Strykowski, P. J.; and Niccum, D. L.: "The Stability of Countercurrent Mixing Layers in Circular Jet," *Journal of Fluid Mechanics*, vol. 227, 1991, pp. 309-343.

24. Strykowski, P. J.; and Wilcoxon, R. K.: "Mixing Enhancements Due to Global Oscillations in Jets with Annular Counterflow," AIAA Journal, vol 31, no. 3, March 1993, pp. 564-570.

25. Strykowski, P. J.; Krothapalli, A.; and Wishart, D.: "Enhancement of Mixing in High-Speed Heated Jets Using a Counterflow Nozzle," *AIAA Journal* vol. 31, no. 11, November 1993, pp. 2033-2038.

26. Olsen, R. E.: "Reattachment of a Two-Dimensional Compressible Jet to an Adjacent Flat Plate," *ASME Symposium on Fluid Jet Control Devices*, 28 November 1962, pp. 23 - 31.

27. Comparin, R. A.; et. al.: "On the Limitations and Special Effects in Fluid Jet Amplifiers," *ASME Symposium on Fluid Jet Control Devices*, 28 November 1962, pp. 65 - 73.

28. Van Der Veer, Michael R.: *Counterflow Thrust Vectoring of a Subsonic Rectangular Jet*. M. S. Thesis, University of Minnesota, Minneapolis, MN, 1995.

29. Strykowski, P. J.; Krothapalli, A.; and Forliti, D. J.*: Counterflow Thrust Vectoring of Supersonic Jets*. AIAA 96-0115, January 1996.

30. Schmid, Geoffrey F.*: Design and Optimization of a Counterflow Thrust Vectoring System*. M. S. Thesis, University of Minnesota, Minneapolis, MN, 1996.

31. Flamm, Jeffrey D.: *Internal Performance Characteristics of a Nozzle Using Fluidic Counterflow for Thrust Vectoring*. M. S. Thesis, George Washington University, Washington D. C., 1996.

32. *A User's Guide to the Langley 16-Foot Transonic Tunnel Complex, Revision 1.* NASA TM-102750, 1990. (Supersedes NASA TM-83186)

33. Berrier, Bobby L.; Leavitt, Laurence D.; and Bangert, Linda S.: *Operating Characteristics of the Multiple Critical Venturi System and Secondary Calibration Nozzles Used for Weight-Flow Measurements in the Langley 16-Foot Transonic Tunnel.* NASA TM-86405, 1985.

34. Mercer, Charles E.; Berrier, Bobby L.; Capone, Francis J.; Grayston, Alan M.: *Data Reduction Formulas for the 16-Foot Transonic Tunnel NASA Langley Research Center*. NASA TM-1076467, July 1992.

35. Panitz, T.; and Wasan, D. T.: Flow Attachment to Solid Surfaces: The Coanda Effect. *AIChE J*., vol. 18, no. 1, Jan. 1972, pp. 51-57.

36. Berrier, Bobby L.: *Results From NASA Langley Experimental Studies of Multiaxis Thrust Vectoring Nozzles*. SAE Tech. Paper SER. 881481, Oct. 1988.

37. Re, Richard J.; and Leavitt, Laurence D.: *Static Internal Performance Including Thrust Vectoring and Reversing of Two-Dimensional Convergent-Divergent Nozzles.* NASA TP-2253, 1984.

38. Mason, Mary L.; and Berrier, Bobby L.: *Static Investigation of Several Yaw Vectoring Concepts on Nonaxisymmetric Nozzles.* NASA TP-2342, 1985.

39. Hunter, Craig, A.; and Wing, David J.*: Counterflow Thrust Vectoring control Volume Analysis.* Unpublished white paper received via personal communication with Craig A. Hunter, August 1995.

40. Coleman, Hugh W.; and Steel, W. Glenn*: Experimentation and Uncertainty Analysis for Engineers.* John Wiley & Sons, 1989.

Component	Balance Maximum	2σ	2σ as percentage of Balance Maximum
Normal	800 lbs	1.40 lbs	0.18
Axial	1200 lbs	0.92 lbs	0.08
Pitch	12000 in-lbs	20.42 in-lbs	0.17
Roll	1000 in-lbs	54.85 in-lbs	5.49
Yaw	12000 in-lbs	23.67 in-lbs	0.20
Side	800 lbs	1.69 lbs	0.21

Table 1. Balance accuracy (95% confidence level).

NPR (nominal)	NPR	δp (deg)	F_r/F_i	w_p/w_i	Δp_{slot} (psi)	w_s (lb/sec)
3.5	±0.004	±0.041	±0.002	±0.002	±0.017	±0.003
4.0	±0.004	±0.043	±0.002	±0.002	±0.017	±0.003
5.0	±0.005	±0.033	±0.002	±0.002	±0.017	±0.003
6.0	±0.006	±0.042	±0.002	±0.002	±0.017	±0.003
6.5	±0.007	±0.041	±0.002	±0.002	±0.017	±0.003
8.0	±0.008	±0.044	±0.002	±0.002	±0.017	±0.003
10.0	±0.010	±0.026	±0.002	±0.002	±0.017	±0.003

Table 2. Uncertainty of computed data (95% confidence level).

G design (in)	G measured (in)	Suction Collar (%)	NPR						
			10	8	6.5	6	5	4	3.5
0.476	0.459	100	✓	✓		✓			
0.238	0.222	100	✓	✓		✓			
0.119	0.110	100	✓	✓	✓				
0.476	0.469	50t	✓	✓		✓	✓	✓	
0.238	0.222	50t	✓	✓		✓	✓	✓	
0.119	0.110	50t	✓	✓		✓	✓		
0.476	0.464	50s	✓	✓		✓	✓	✓	✓
0.238	0.223	50s	✓	✓		✓	✓	✓	✓

s =scaled
t = truncated

Table 3. Test matrix. Δp_{slot} varied at each NPR.

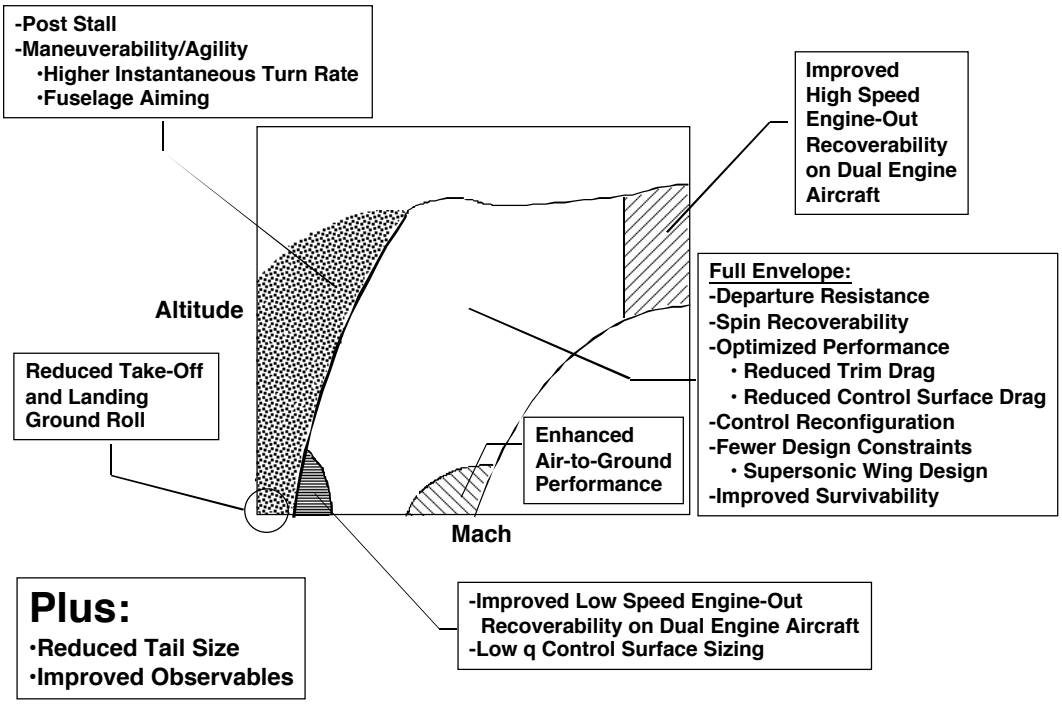

Figure 1. Potential Benefits of Thrust Vectoring.

Figure 2. F-18 HARV Thrust Vectoring Nozzles.

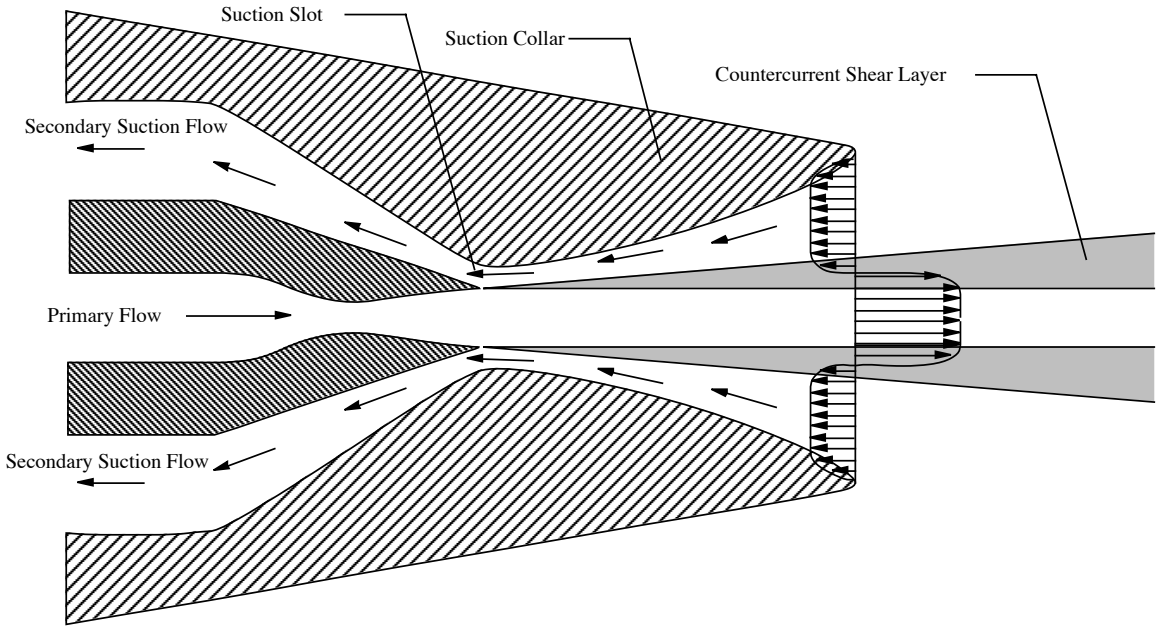

Figure 3. Generation of Countercurrent Shear-Layers.

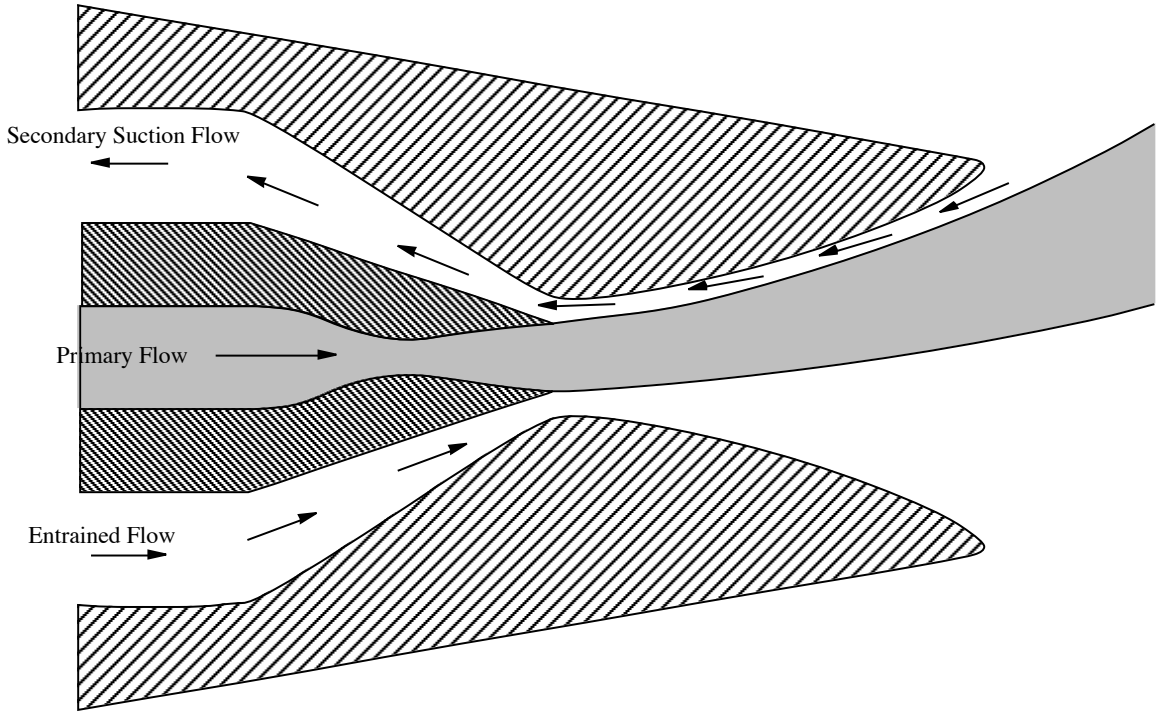

Figure 4. Asymmetric Suction for Thrust Vectoring.

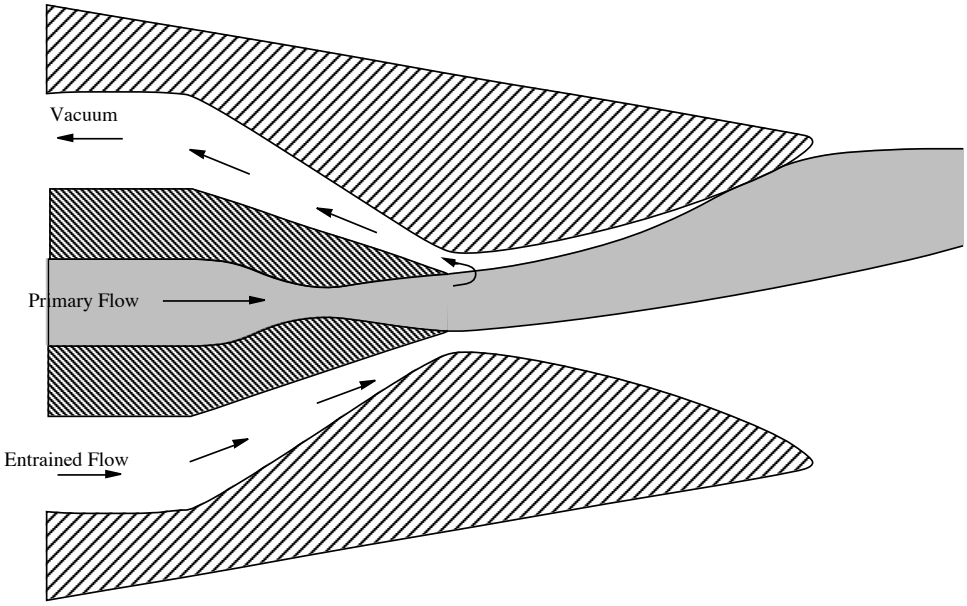

Figure 5. Jet Attachment.

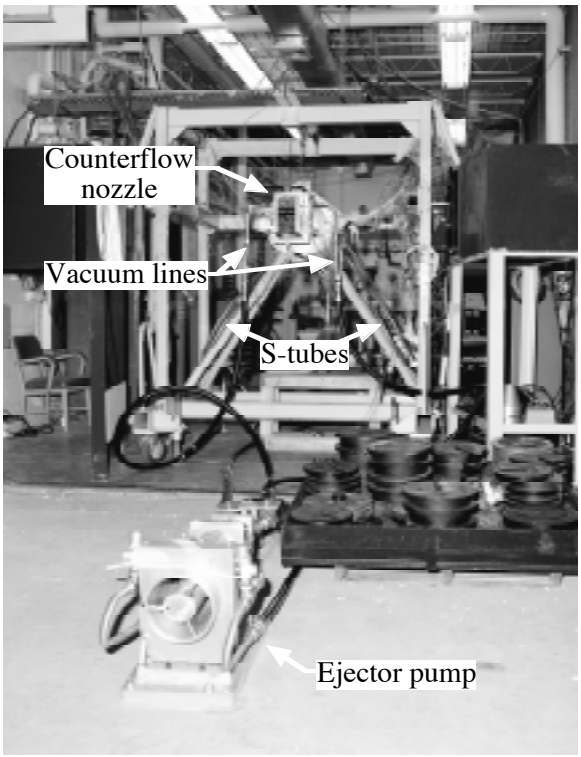

Figure 6. Counterflow Nozzle Installed in the Jet Exit Test Facility.

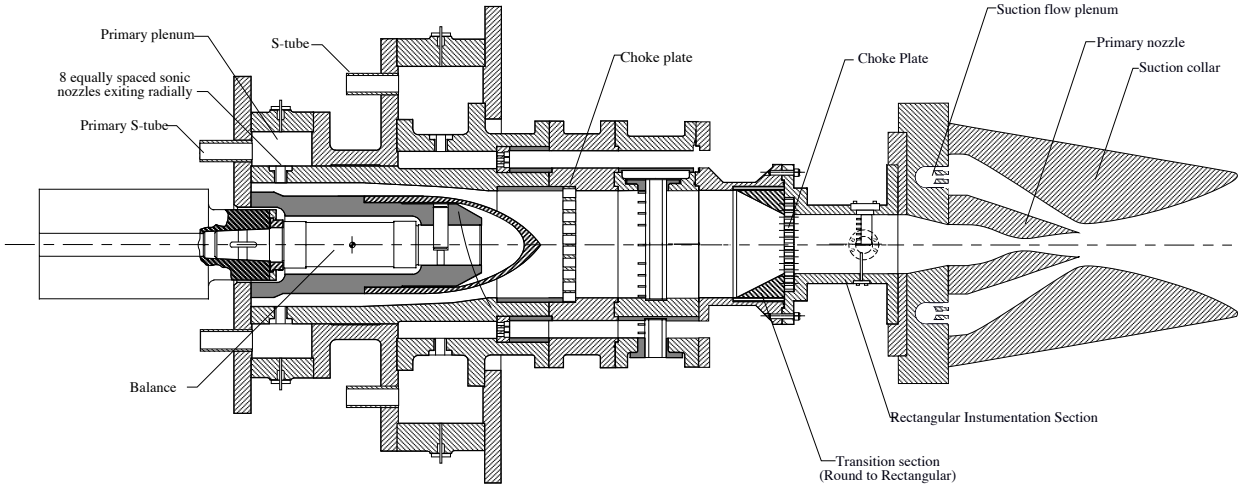

Figure 7. Cross-Section of Counterflow Thrust-Vectoring Nozzle on Dual-Flow Propulsion Simulation System.

Collar	L (in)	G (in)	H (in)	C (in)	θ (deg)	A_e/A_t
100%	7.957	0.459	1.125	2.246	27.8	1.688
100%	↓	0.222	↓	↓	↓	↓
100%	↓	0.110	↓	↓	↓	↓
50% truncated	3.979	0.469	↓	0.572	15.8	↓
50% truncated	↓	0.222	↓	↓	↓	↓
50% truncated	↓	0.110	↓	↓	↓	↓
50% scaled	↓	0.464	↓	1.090	27.8	↓
50% scaled	↓	0.223	↓	↓	↓	↓

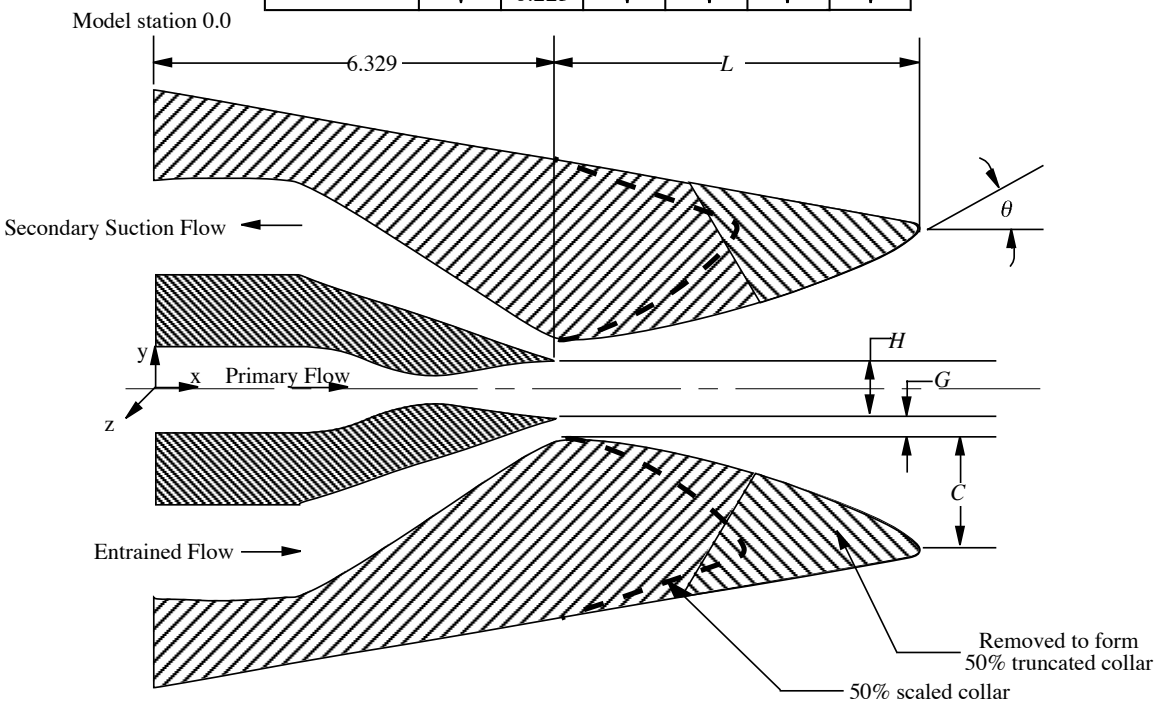

Figure 8. Sketch of Counterflow Nozzle (Width, $W = 4.5$ in).

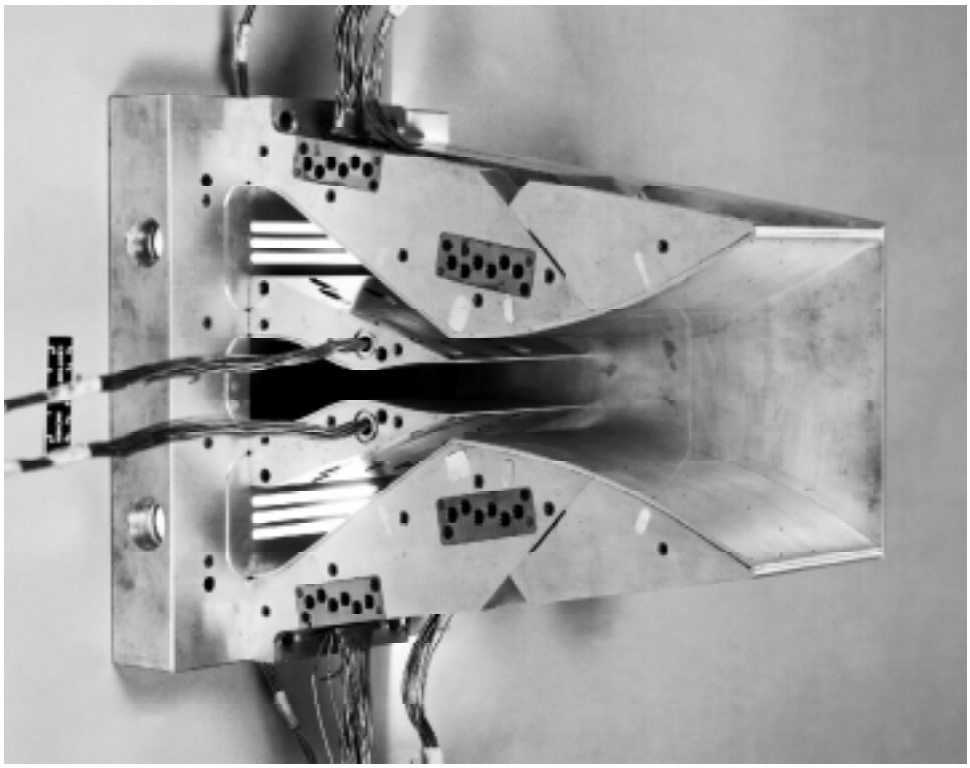

Figure 9. Typical Nozzle Configuration, 100% Collar, G = .459 in. (sidewall removed).

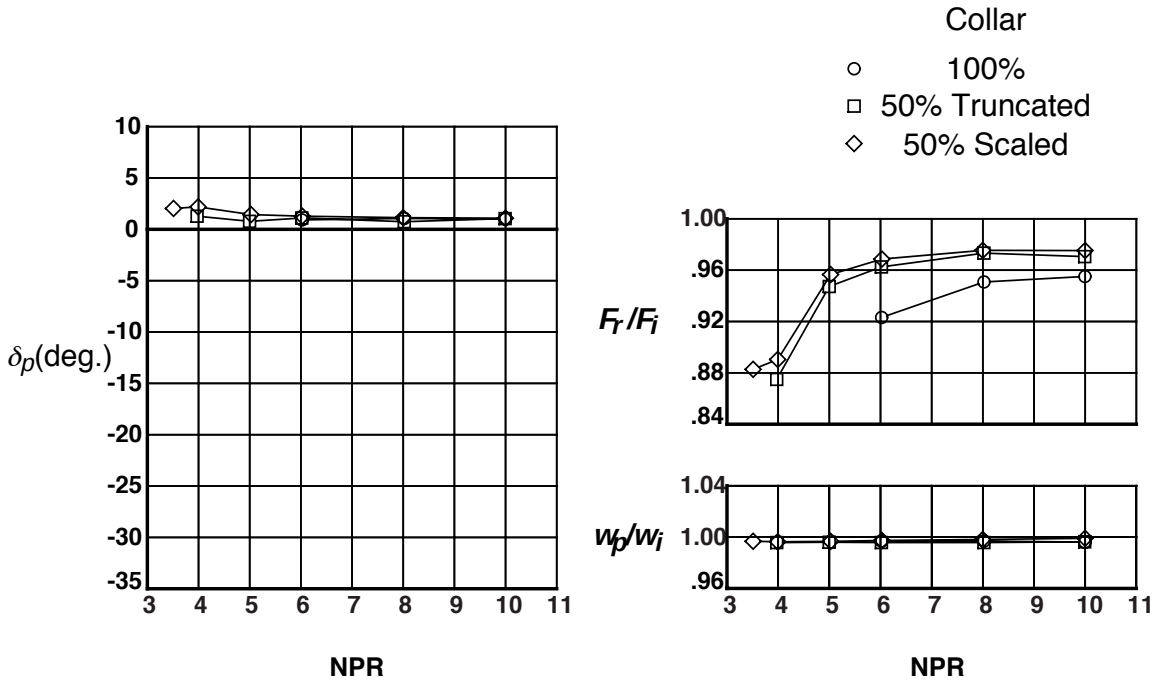

Figure 10. Effect of Collar Geometry on Nozzle Performance, G = 0.465 in., No Counterflow.

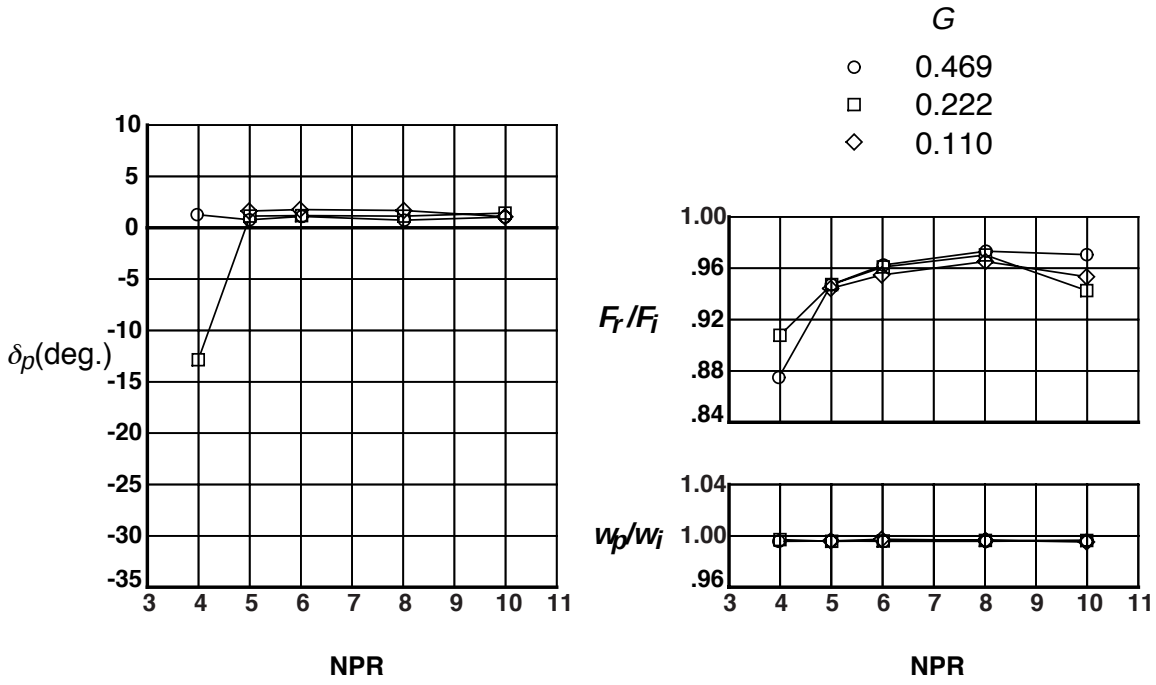

Figure 11. Effect of Suction Slot Height on Nozzle Performance, 50% Truncated Collar, No Counterflow.

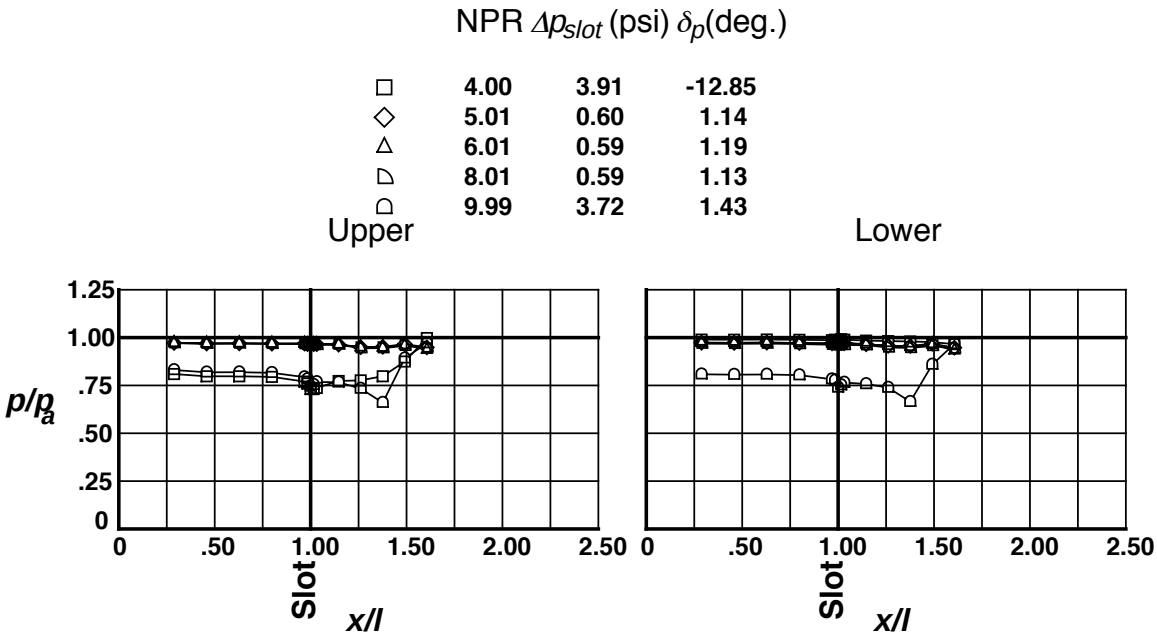

Figure 12. Suction Collar Internal Centerline Pressure Distribution, 50% Truncated Collar, G = 0.222 in., No Counterflow.

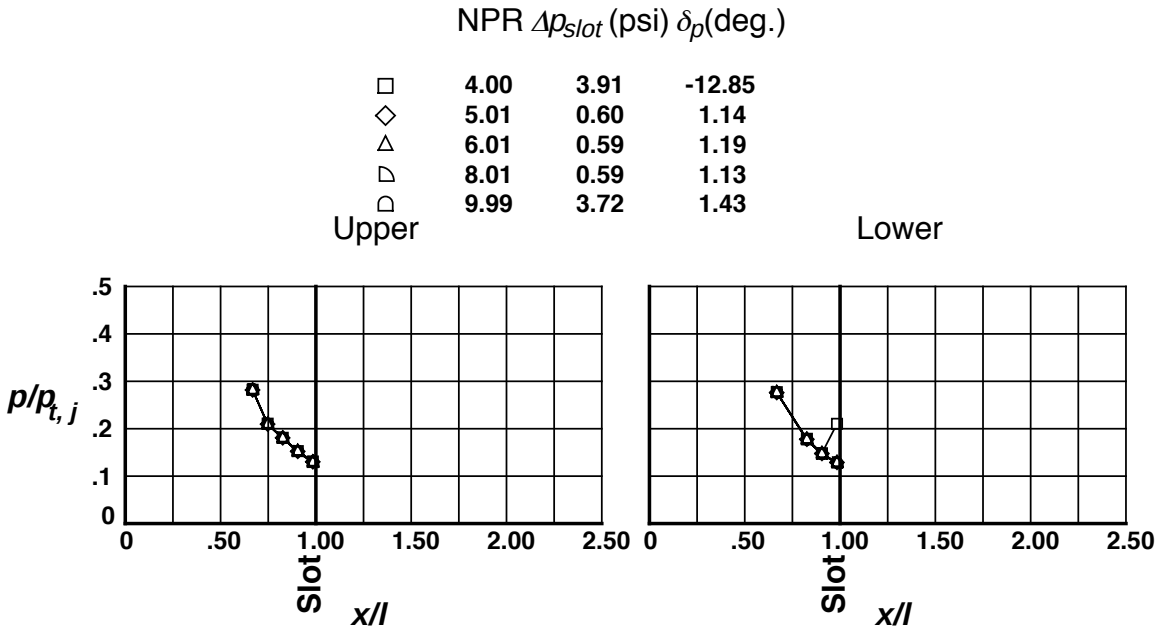

Figure 13. Primary Nozzle Internal Centerline Pressure Distibution, 50% Truncated Collar, G = 0.222 in., No Counterflow.

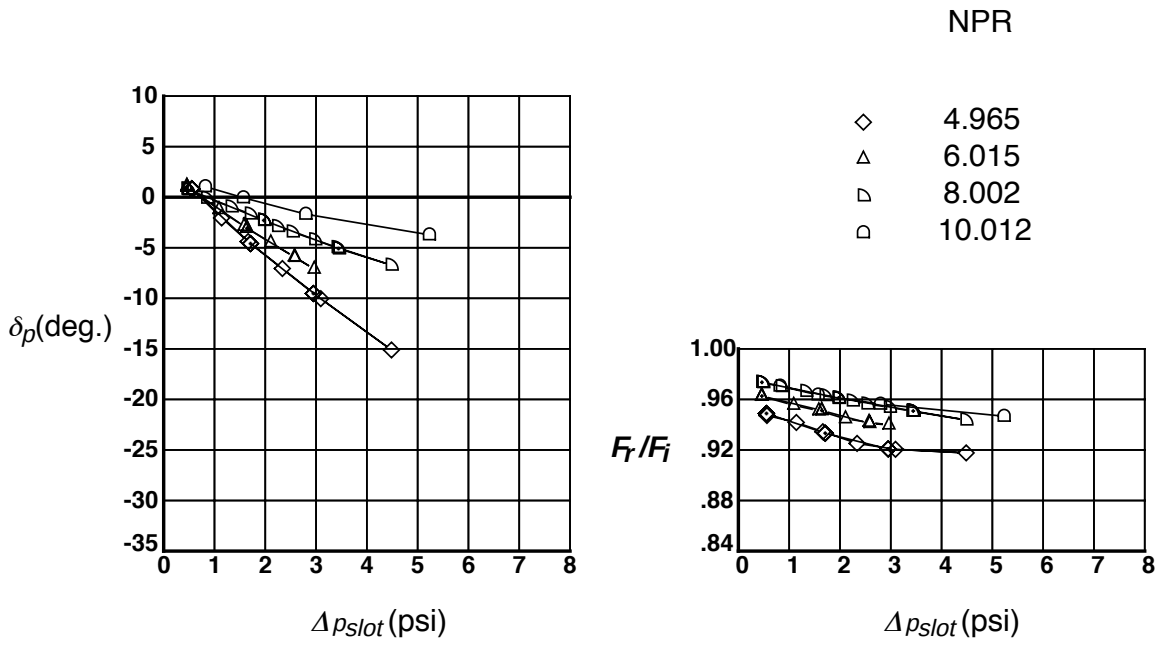

Figure 14. Effect of NPR on Nozzle Performance, 50% Truncated Collar, G = 0.469 in., Counterflow on.

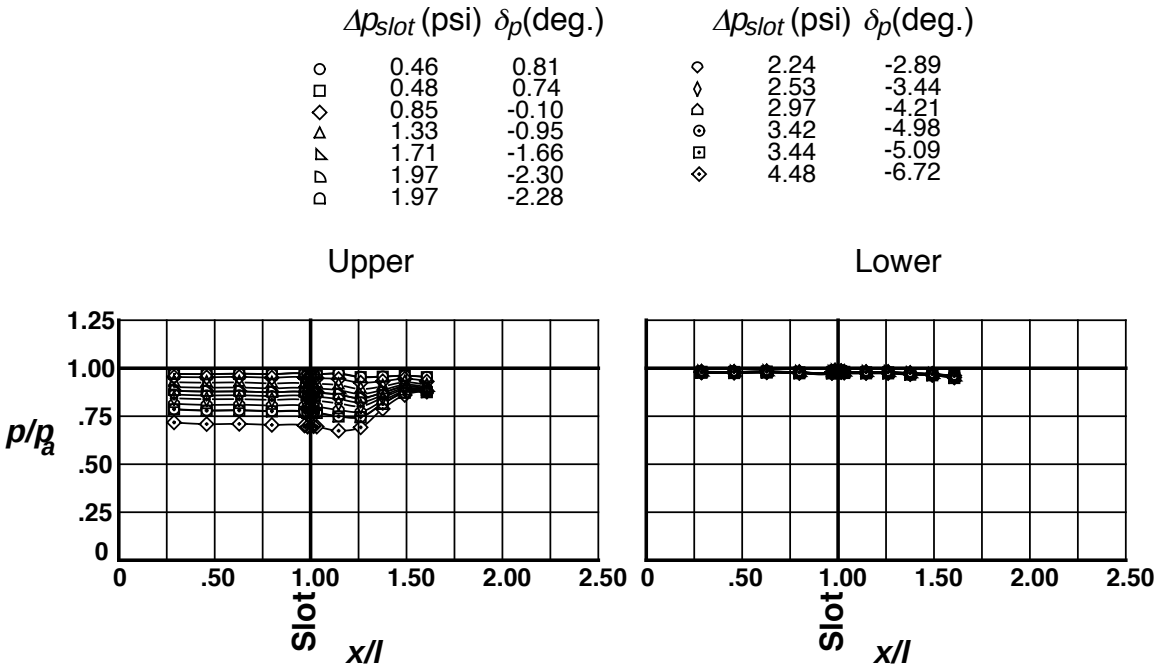

Figure 15. Typical Suction Collar Centerline Pressure Distribution, 50% Truncated Collar, G = 0.469 in, NPR=8.0, Counterflow on.

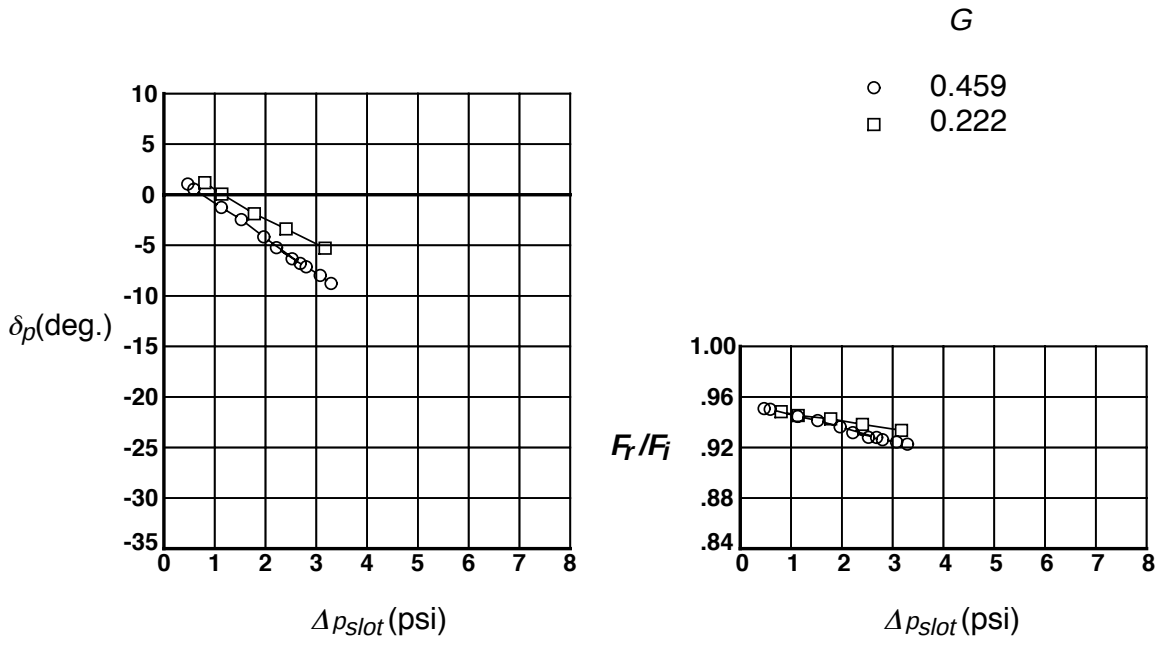

Figure 16. Effect of Slot Height on Nozzle Performance, 100% Collar, NPR = 8.0, Counterflow on.

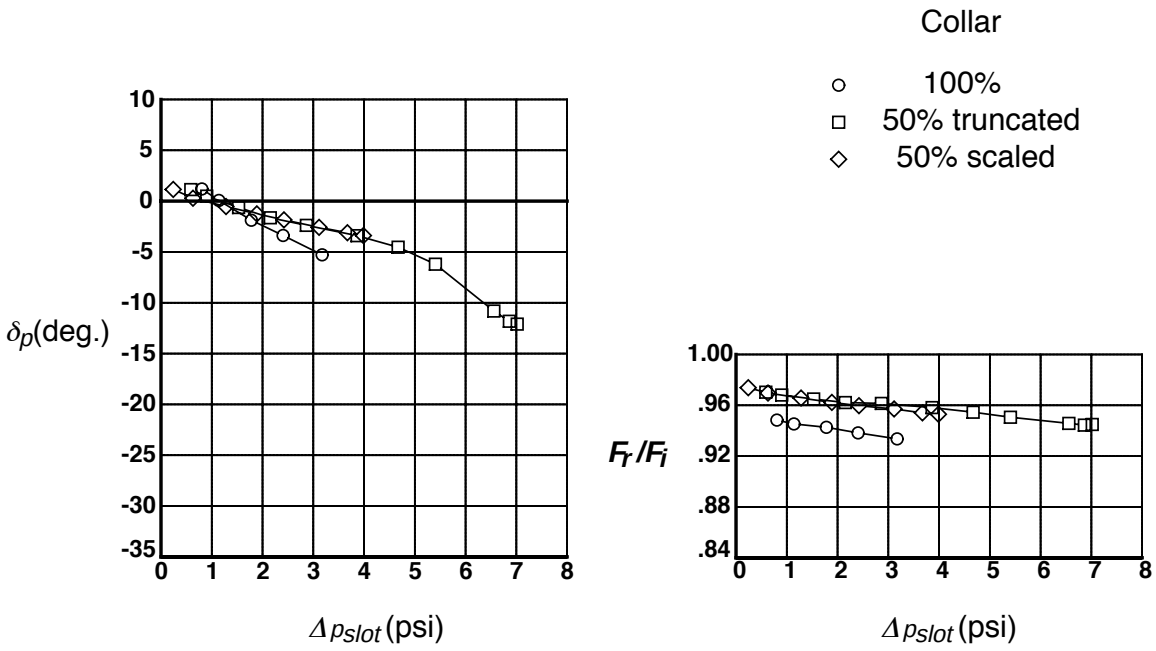

Figure 17. Effect of Collar Geometry on Nozzle Performance, G = 0.222 in., NPR = 8.0, Counterflow on.

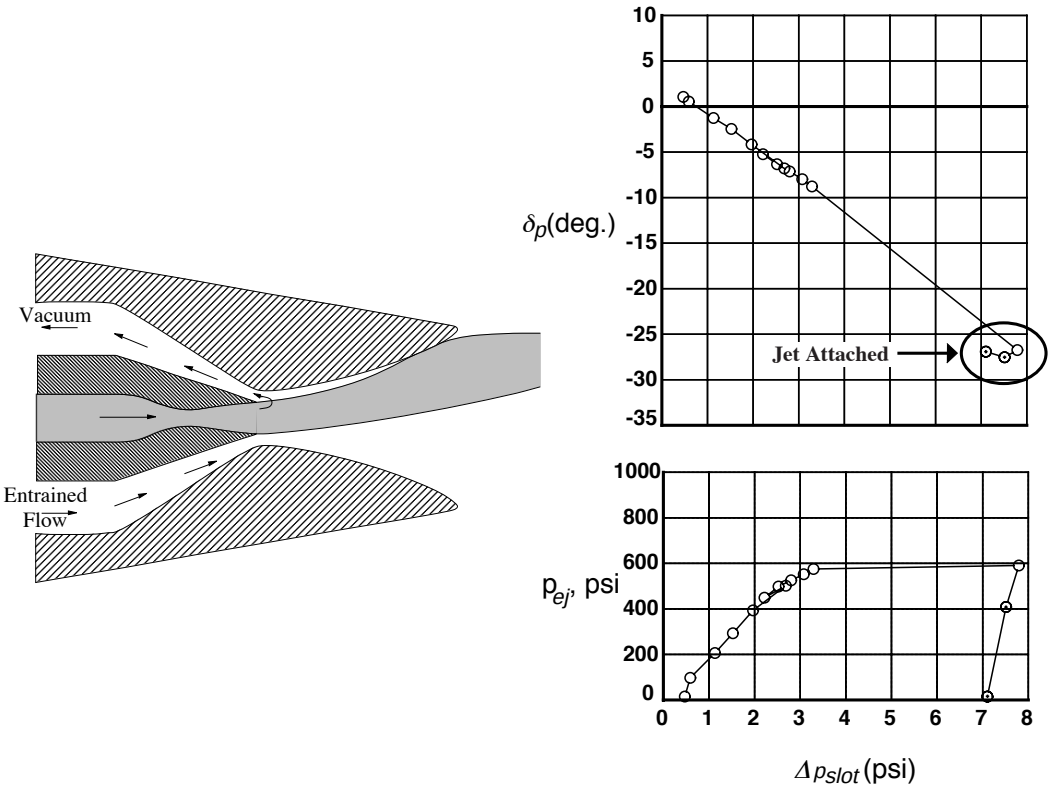

Figure 18. Jet Attached to One Collar, 100% Collar, G = 0.459 in., NPR = 8.0, Counterflow on (+ symbol indicates data taken in descending order of Δp_{slot}).

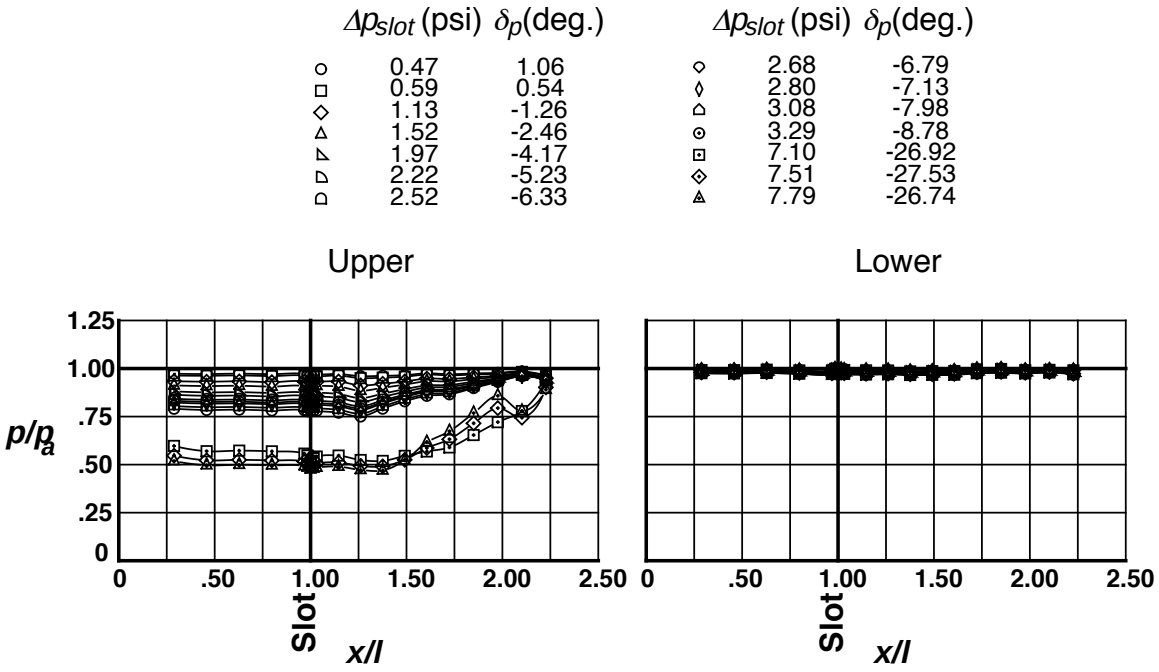

Figure 19. Suction Collar Centerline Pressure Distribution - Jet Attached to One Collar, 100% Collar, G = 0.459 in., NPR = 8.0, Counterflow on.

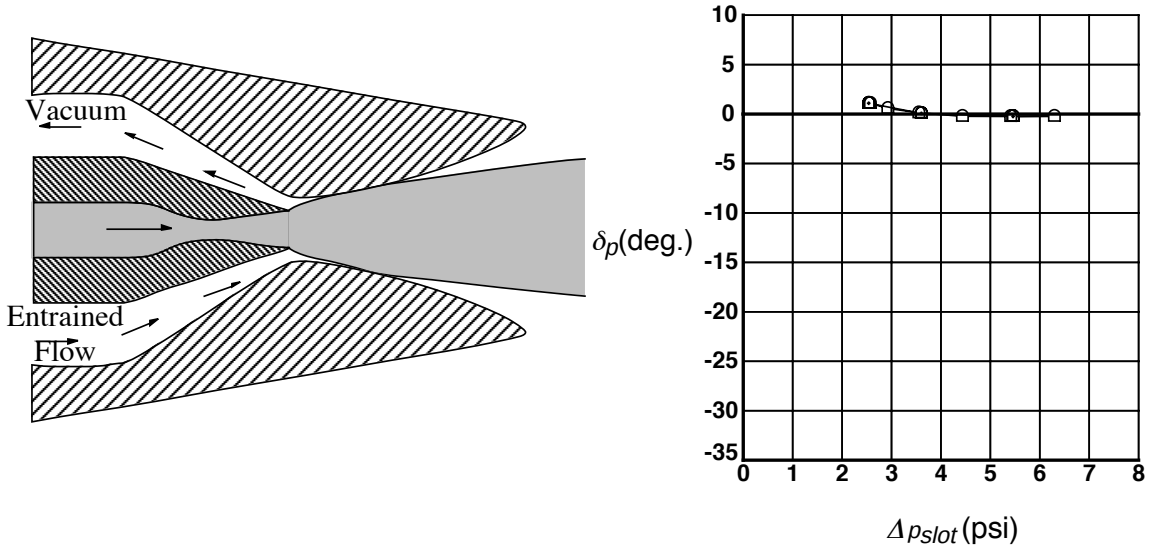

Figure 20. Jet Attached to Both Collars, 100% Collar, G = 0.110 in., NPR = 10.0, Counterflow on.

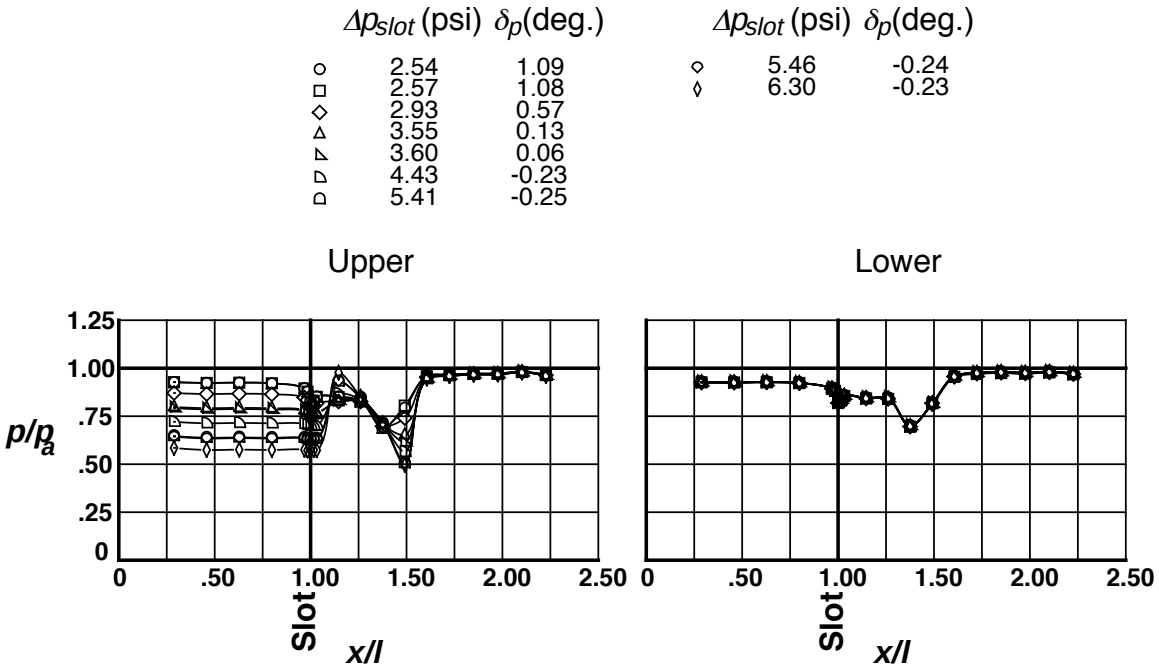

Figure 21. Suction Collar Centerline Pressure Distribution - Jet Attached to Both Collars, 100% Collar, G = 0.110 in., NPR = 10.0, Counterflow on.

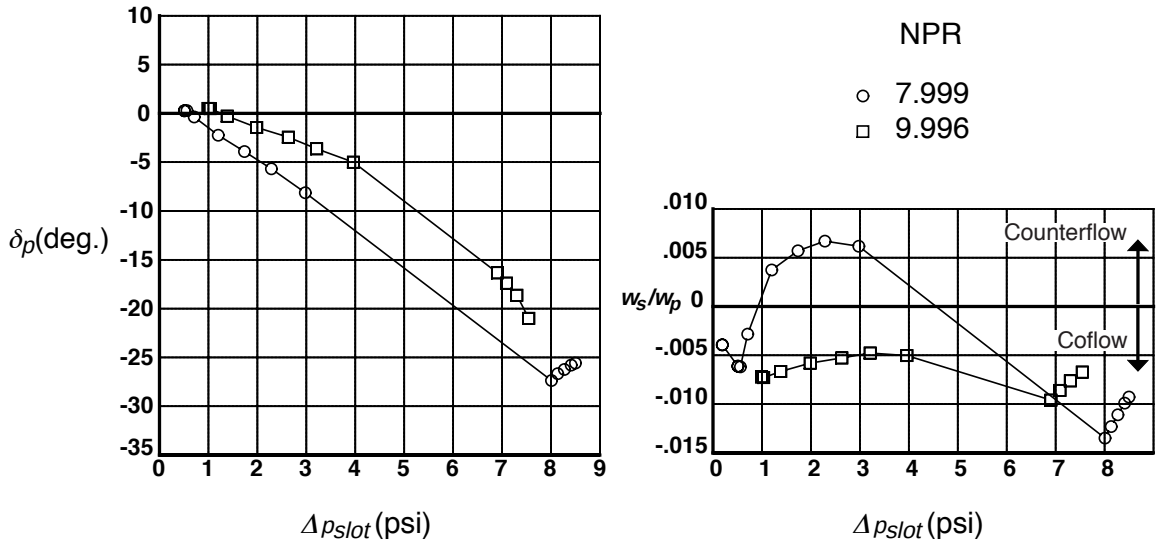

Figure 22. Secondary (vacuum) weight flow measurements, 100% Collar, G = 0.459 in., Counterflow on.

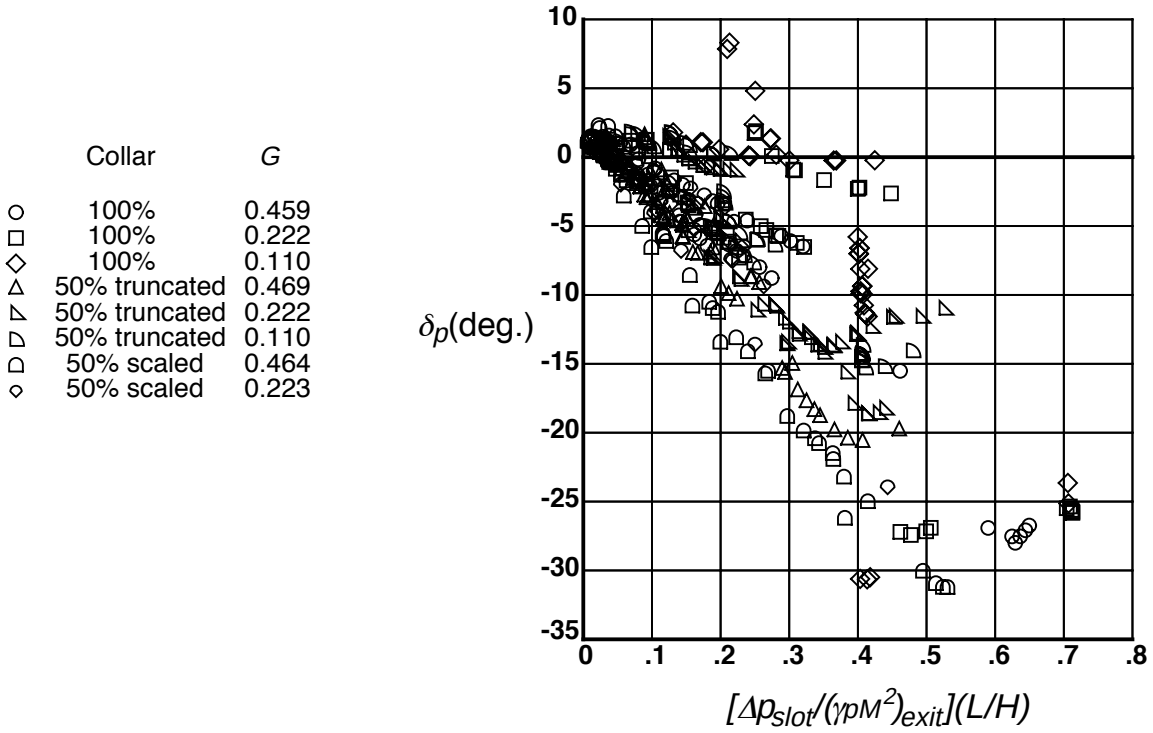

Figure 23. Experimental data plotted against the Van Der Veer parameter (reference 28).

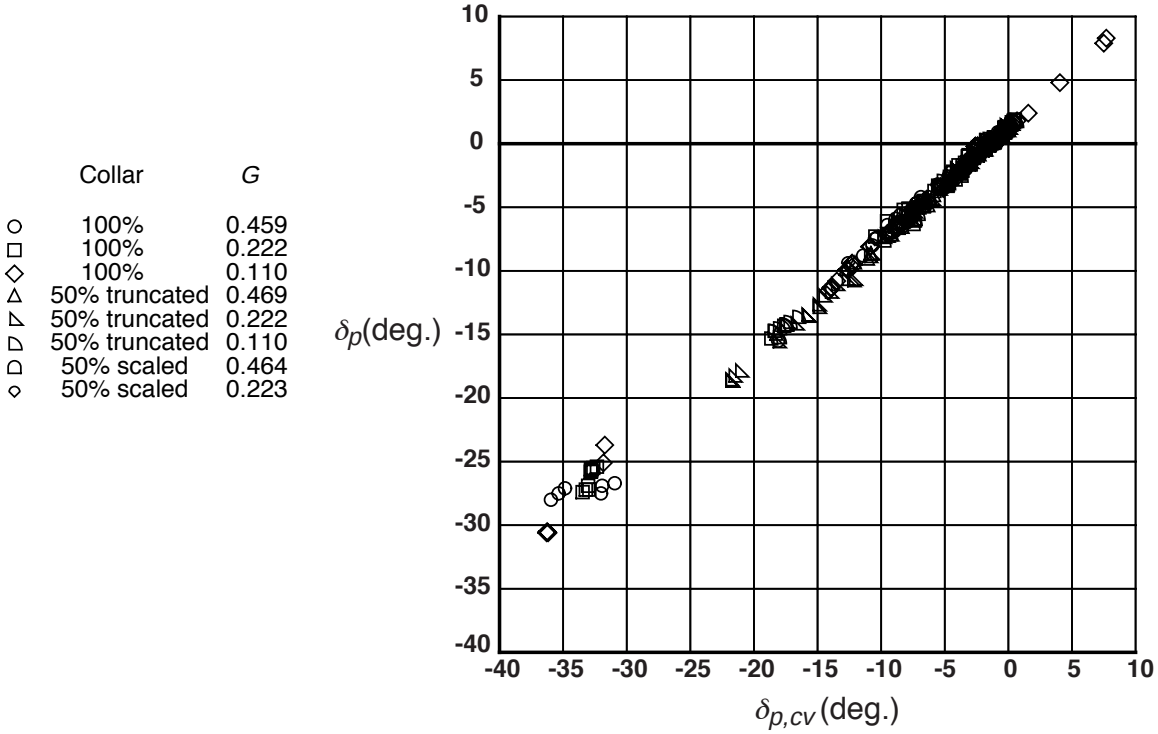

Figure 24. Data correlation with full control volume analysis, NPR > 4.0.

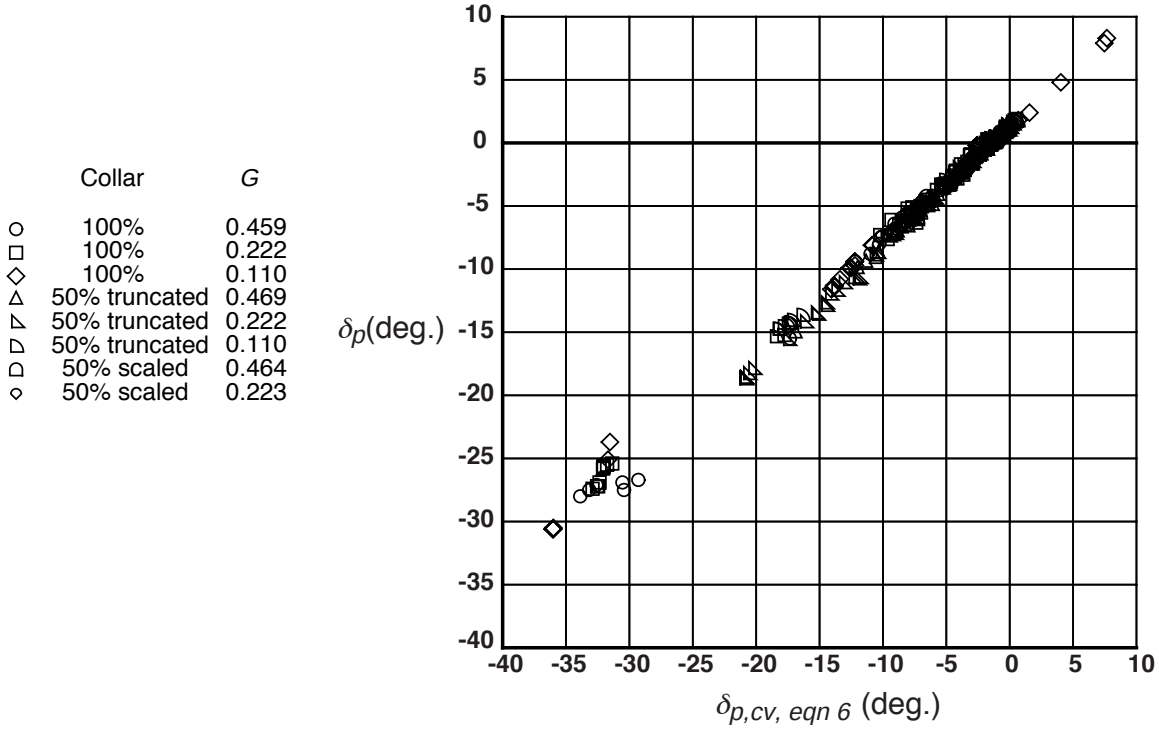

Figure 25. Data correlation with simplified control volume analysis, NPR > 4.0.